Size matters: gold nanoparticles in targeted cancer drug delivery

Erik C Dreaden[1], **Lauren A Austin**[2], **Megan A Mackey**[2], and **Mostafa A El-Sayed**[2,*]

[1]The David H Koch Institute for Integrative Cancer Research, Massachusetts Institute of Technology, 77 Massachusetts Avenue, Cambridge, MA 02139, USA

[2]Laser Dynamics Laboratory, Department of Chemistry & Biochemistry, Georgia Institute of Technology, 901 Atlantic Drive NW, Atlanta, GA 30332-0400, USA

Abstract

Cancer is the current leading cause of death worldwide, responsible for approximately one quarter of all deaths in the USA and UK. Nanotechnologies provide tremendous opportunities for multimodal, site-specific drug delivery to these disease sites and Au nanoparticles further offer a particularly unique set of physical, chemical and photonic properties with which to do so. This review will highlight some recent advances, by our laboratory and others, in the use of Au nanoparticles for systemic drug delivery to these malignancies and will also provide insights into their rational design, synthesis, physiological properties and clinical/preclinical applications, as well as strategies and challenges toward the clinical implementation of these constructs moving forward.

Nanoparticles – materials with dimensions between 10^{-9} and 10^{-8} m – have been systemically administered in humans since clinical approval of the first micellar drug Sandimmune® by the US FDA in 1983 and the first polymer–drug nanoconjugate Adagen® later, in 1990 [1]. Since then, an explosion of research in nanoscale diagnostic and therapeutic agents has given rise to a range of biomedical nanotechnologies and platforms [2–9], including protein–drug nanoconjugates [10], micelles [11–14], liposomes [15,16], dendrimers [17–19], inorganic nanoparticles [8,20–27] and other polymer–drug nanoconjugates [2,28–31] (Supplementary Table 1). Approximately over two dozen biodiagnostic or therapeutic nanotechnologies have been approved for clinical use with 250 others in clinical development. The global market share for biomedical nanotechnologies is expected to grow to US$70–160 billion by 2015, potentially rivaling the current worldwide market for biologics [32]. These nanoscale constructs provide a range of multiple, fundamentally new properties, which can be exploited in ways that can improve our ability to detect, treat and monitor disease states. Further, the unique interactions between these nanoscale materials and comparably sized physiological structures, proteins, organelles and DNA, for example, can also be leveraged to compliment existing medical diagnostic/treatment strategies and to foster the development of new and potentially more efficacious approaches.

*Author for correspondence: Tel.: +1 404 894 0292, Fax: +1 404 894 4066, melsayed@gatech.edu.

Gold (Au) nanoparticles (AuNPs) exhibit a combination of physical, chemical, optical and electronic properties unique from other biomedical nanotechnologies and provide a highly multifunctional platform with which to image and diagnose diseases [33–37], to selectively deliver therapeutic agents [34,38–40], to sensitize cells and tissues to treatment regimens [41,42], to monitor and guide surgical procedures [23,43,44], and to preferentially administer electromagnetic radiation [45–48] to disease sites (Figure 1). Owing to their large size, circulating nanoparticles preferentially accumulate at tumor sites and in inflamed tissues due to the characteristically defective architecture of the vessels that supply oxygen and nutrients to these tissues [49,50]. Once circulating nanoparticles extravasate through these large vascular pores and into the disease site, they remain lodged due to characteristically diminished lymphatic drainage and their low diffusivity [51]. First termed by Maeda and Matsumura in 1986 [52,53], the **enhanced permeability and retention (EPR) effect** provides a basis for the selective accumulation of many current high-molecular-weight drugs currently in clinical use. AuNPs can be used to deliver drugs and imaging agents that otherwise exhibit low solubility and poor pharmacokinetics [54,55]. These platforms can deliver compounds that are intrinsically susceptible to enzymatic degradation, as well as those that exhibit poor intracellular penetration (e.g., siRNA) [39,56–58]. AuNPs can be routinely surface functionalized with active ligands at densities ($1.0 \times 10^6 \ \mu m^{-2}$) [59] that are 100- and 1000-fold higher than that achievable with conventional liposomes [60] or poly(lactic-co-glycolicacid) nanoparticles [61], respectively, allowing their binding affinity [62] to be optimized for a particular disease type, stage or patient. Because of their comparability in size to the distances between cell-surface targets, Au nanostructures can simultaneously engage multiple, adjacent receptor sites, achieving increased selectivity in their uptake through this multivalent **avidity** [63].

The novel optical and electronic properties of AuNPs are particularly attractive for use in multimodal drug-delivery applications where these structures can afford enhanced drug pharmacokinetics/biodistribution and simultaneous **hyperthermia** [8,22,46,47,64,201] and radiation therapy contrast [41,44,65–68], as well as photo-imaging contrast [33,35,44,65,69–76], spectrochemical diagnostic contrast [34,37,43,77–79] and, when molecularly directed to specific subcellular sites, intrinsic pharmacodynamic properties [8,9,80]. The ability of these structures to act as photothermal therapeutic agents arises due to the delocalized nature of their free (conduction) electrons and the increasing polarizability of these charge carriers at the surfaces of these materials. These surface electrons exhibit collective modes of oscillation (surface plasmon modes), which vary in frequency depending on the size/shape of the nanoparticle and its dielectric environment [81]. Plasmon modes that result in a dipolar charge density distribution can couple with and resonantly absorb optical photons of the same frequency, resulting in a transient increase in the energy of these electrons equivalent to that of the photon (E_{Fermi} [Au] ~−5.1 eV v. Evac) [82]. Plasmonic photothermal heat generation [83] can thus be simplified as a three-step process: electron–electron coupling; electron–phonon coupling; and phonon–phonon coupling. Electron–electron coupling follows the energy absorption process, whereby the average (Fermi) energy of electrons in the nanoparticle is transiently increased for a few hundred femtoseconds. This increased electron energy decays via the coupled electronic and lattice heat capacities of the material (i.e., energy per unit temperature), resulting in a transient (~1 ps) increase in the material's lattice temperature and, thus, an increase in the volume of the nanoparticle. Volume expansion equilibrates through phonon 'breathing' modes (phonon–phonon coupling), whereby coherent oscillations of the atomic lattice (phonon vibrations) dissipate energy, resulting in heat transfer to the surrounding media over several picoseconds. The extent of macroscopic heat generation depends on the incident excitation power and the particle, but, in most *in vivo* therapeutic applications, photothermal heat increases often exceed 20°C [8,9,45–48,64,84]. By changing the size/shape/surface of the AuNP, one can tune the wavelength of its plasmon absorption to coincide with spectral

regions where the attenuation of photons by tissues and physiological fluids (i.e., water and oxy/deoxyhemoglobin) is minimal [8,85]. For example, in the **near-IR (NIR) window** (~650–900 nm), one can achieve upwards of 10 cm penetration depth through breast tissue even at low ($\mu W/cm^2$) laser power densities [8,9,86]. The local temperature increases attainable using laser **photothermal therapy** (PTT) are sufficient to induce rapid tumor cell death (necrosis) with minimal damage to surrounding tissues. In milder, hyperthermic cases (ΔT~3–5°C) [87], deleterious physiological responses such as cell membrane disruption, protein denaturation, metabolic signaling disruption, thrombosis, tumor ischemia, the induction of heat-shock proteins, signaling disruption, diminished membrane transport and impaired DNA synthesis/repair can also lead to pro-apoptotic responses in particle-labeled cancer cells [88,89]. Since AuNPs are comprised of a high atomic number (i.e., high-Z) element, they have been shown to substantially to improve the efficacy of radiotherapy treatments via tumor-localized photoelectron and Auger electron ejection, which can damage the DNA of tumor cells in the local surrounding tissue [41]. Hyperthermia is also known to synergize with radiotherapy treatments [90]; however, reports of multimodal plasmonic laser PTT and high-Z enhanced radiotherapy using AuNPs have yet to be explored.

Synthesis & conjugation of biomedical AuNPs

Systemically deliverable AuNPs are most often synthesized by colloidal methods, whereby a solution of Au salt is chemically reduced in the presence of surface stabilizers, which prevent aggregation of the formed Au solution as a consequence of attractive Van der Waals and depletion forces [91]. In most cases, spherical AuNPs are well suited for drug-delivery applications due to the fact that they can be synthesized on a large-scale with high monodispersity (Figure 2A). Unlike most AuNPs of complex geometry, spherical nanogold can be synthesized using highly labile stabilizing ligands that allow for facile, efficient and high-density ligand exchange. For example, the bond strength between the Au surface and citrate anions [92] used in the common Turkevich/Frens method [93,94] is comparable to that of a hydrogen bond and, is thus, easily displaced by more strongly bound thiols [95] or amines [92]. Colloidal synthetic methods are often thought to follow a semi-Lamer growth process, where chemical reduction of metal salt results in spontaneous particle nucleation and subsequent isotropic particle growth. In contrast, the Turkevich/Frens method proceeds via four overlapping steps: nucleation; aggregation of nuclei; slow isotropic growth via reduction and/or coalescence/Ostwald ripening [96]; and rapid consumption of the Au precursor [97]. Mechanistically, Au reduction occurs through a concerted redox reaction, whereby citrate is both chemically oxidized by chloroauric acid and thermally oxidized by heating to form dicarboxyacetone (DCA) [98–100]. Electrons from DCA serve to reduce $AuCl_3$ to $AuCl$, which is believed to form a bidentate complex with DCA. Particle nuclei form via a disproportionation reaction, where AuCl complexes combine to form zero-valent Au atoms and an $AuCl_3$ complex. Here, particle size is generally adjusted by varying the Au salt: citrate ratio or reaction pH [98,101]. Smaller AuNPs are often synthesized via Brust–Schriffrin reduction of AuCl [102]. In this method, Au salt is dissolved in toluene by way of a phase-transfer catalyst (e.g., tetraoctylammouium bromide) and borohydride is added to an aqueous phase of the reaction mixture, forming Au clusters in the organic phase stabilized by co-solvated alkanethiols. Although these particles exhibit novel molecule-like properties, their use in biomedical application is typically limited to immunolabeling [103], x-ray imaging [36] and radiotherapy [104] applications due to reported toxicity [105] at these sizes.

In applications where photothermal heating/delivery or NIR excitation is desired, rod-shaped AuNPs, as well as hollow and core–shell nanostructures are employed (Figure 2B). Interested readers are directed to Dreaden *et al.* for a more thorough review of the synthesis

and applications of biomedically relevant Au nanostructures [9]. Au nanorods (AuNRs), a particular focus of our group, are synthesized by a seeded growth method developed by Murphy and co-workers, and Nikoobakht and El-Sayed [106,107]. Briefly, small (~1.5 nm diameter) seed nanoparticles are formed via classical borohydride reduction of Au salt in the presence of a cationic surfactant stabilizer. These seeds are then added to a solution containing additional surfactant and Au salt that has been mildly reduced by ascorbic acid, forming dehydroascorbic acid and resulting in an $AuCl_2^-$–surfactant complex [108]. Collisions between the Au(I) complex and the seed particles, together with contributions from surface-adsorbed halide ions, silver ions and crystallographically preferential surfactant adsorption, results in the anisotropic growth of AuNRs approximately 10–20 nm in width and up to 300 nm in length, depending on the specific synthetic conditions employed [109]. Readers may wish to note that the bonding interaction between Au and cetyltrimethylammonium bromide (CTAB) is atypical of almost all chemical conjugation schemes involving AuNPs. Br^- anions are known to form atomic surface layers on Au and other metals/semiconductors (i.e., adlayers) and also form electrostatically coordinate CTA^+ cations and their micelles. The general consensus for AuNR–CTAB bonding involves the formation of a Br^- adlayer on the AuNR surfaces which then coordinates N headgroups on CTA^+. The aliphatic tail of surface-bound CTA^+ then associates with another CTA^+ cation oriented with its N^+Br^- headgroup facing outwards [110].

Due to their ability to participate in noncovalent and covalent/dative bonding, AuNPs can undergo facile surface chemistry. Once synthesized, the AuNP surface is surrounded by a stabilizing agent, which creates an overall surface charge. These stabilizing agents offer the possibility of conjugating a variety of biomolecules such as DNA, antibodies and polypeptides through electrostatic interactions. McIntosh *et al.* utilized mixed monolayer protected Au clusters coated with a cationic stabilizing agent, 11-trimethylammoniumundecanethiol, to non-covalently attach the negatively charged phosphate backbone of DNA to the surface of the nanoparticle [111]. UV-visible spectroscopy and dynamic light scattering indicated that DNA conjugation to mixed monolayer protected Au clusters did not induce instability or aggregates in the conjugated solution. Huo and co-workers demonstrated that anionic, citrate-stabilized Au nanospheres could be successfully coupled with prostate-specific antigen antibodies through electrostatic interactions [112]. Here, conjugation was confirmed by the 20-nm increase in the **hydrodynamic diameter** (HD) of the nanosphere after coupling.

Although noncovalent bonding provides a relatively easy mode of conjugation, coupling ligands to the surface of AuNPs through covalent or dative bonding also increases conjugate stability, necessary when particles are introduced into environments (e.g., high ionic strength, high serum concentration) that would otherwise cause adverse effects such as aggregation and insolubility. Traditionally, covalent attachment is achieved through a free thiol, amine or carboxylate functional group, allowing for facile conjugation to a variety of biomolecules and biopolymers. Au–S bonds are fairly robust (~40 kcal mol^{-1} [95]), approximately half the strength of a typical C–C or C–H bond; in contrast, Au–N (~8 kcal mol^{-1} [92]) and Au–COO^- (~2 kcal mol^{-1} [92]) dissociation energies are much weaker, comparable to in strength with a hydrogen bond and, thus, easily displaced. One particular advantage of AuNPs is their well-defined, high-density surface structure; while AuNP surfaces [59] can be routinely functionalized with active ligands (i.e., not stabilizers) at densities approximately 1.0×10^6 molecules/μm^2, those typically attainable using more conventional liposomes [113] and poly(lactic-co-glycolic acid) nanoparticles [114] are two-to-three orders of magnitude less – 1.2×10^4 and 4.4×10^6 molecules/μm^2, respectively. Phadtare *et al.* utilized the Au–N bond to conjugate AuNPs to polyurethane microspheres in order to immobilize pepsin [115]. In this study, covalent coupling occurred between the N atoms in polyurethane and the Au atoms on the surface of the nanospheres. While amines

and other N-containing groups are utilized to adhere ligands to the surface of AuNPs, the most common covalent bond and anchoring group is a thiol linker. The Au–S bond is fairly strong (45 kcal/mol) and results from the soft atom characteristics of both Au and S [116]. Stabilizing polymers and biomolecules are often modified to contain an -SH group to enhance their conjugation on the surface of the Au surface. This form of conjugation was utilized by Kang *et al.* to attach **poly(ethylene glycol)** (PEG) to 30-nm AuNPs, which increased the particles' stability in biological environments and allowed for the subsequent conjugation of a nuclear-localizing signal peptide through free thiol groups located at cysteine residues on the peptide [80]. Additionally, linker molecules can be modified to contain a thiol group on one terminal end, which is used to attach to the Au surface and an amine ($-NH_2$) or carboxylic acid ($-COOH$) functional group on the other end. The free functional group allows for drug coupling to the nanoparticle through traditional ethyl(dimethylaminopropyl) carbodimide- and *N*-hydroxysuccinimide-catalyzed cross-coupling (Figure 3).

As stated above, AuNPs are often conjugated to surface molecules that undergo ligand exchange with the particle's capping material and increase particle stability in physiological environments. In biological settings, polymers such as PEG and oligoethylene glycol are commonly used to help minimize nonspecific adsorption of other biomaterials on the particle surface and increase particle stability in high-ionic strength environments, such as cell culture medium and physiological fluids. Biocompatible polymers that exhibit low (positive or negative) surface charge have also minimized the immunogenic response and decreased the recognition of the AuNPs by macrophages and the reticuloendothelial system (RES) [117]. Tong *et al.* have shown that AuNPs conjugated to branched PEG molecules have increased blood circulatory half-life when compared with nanorods conjugated to linear PEG [118]. The increased circulatory half-life was attributed to the extensive surface coverage by the branched PEG ligands, allowing the nanoparticles to evade serum protein binding.

Pharmacokinetics & biodistribution of AuNPs

AuNP-based chemotherapeutics, namely drug delivery, are most effective when certain biological barriers are overcome through nanoparticle design. Clearance by the RES is common in all types of drug-delivery systems, as it occurs through opsonization and is dependent on size; it can be circumvented through coating AuNPs with hydrophilic polymers and decreasing the size of the nanoparticle. Amplified angiogenesis, a hallmark of tumors, causes an increase in the tumor fluid pressure, preventing accumulation of nanoparticles within the tumor interstitium. This barrier can be overcome by utilizing the passive accumulation of AuNPs by extravasation of leaky tumor vasculature afforded by the EPR effect (*vide infra*). Site/cell-specific drug delivery is particularly crucial in nanoparticle drug-delivery systems and can be achieved through the functionalization of AuNPs with both tumor-targeting ligands and therapeutic molecules [119]. In order to design AuNPs as drug-delivery vectors, all of the abovementioned barriers must be considered and many groups have done so by investigating the pharmocokinetics and different targeting strategies for various nanoparticle designs.

In general, the typical size of nanoparticle-delivery systems is between 10 and 100 nm. With this range of nanoparticle size comes a range of pharmacokinetic and biodistribution parameters [120,121]. There have been many accounts of size-dependent blood half-lives and biodistribution profiles for spherical AuNPs as well as rod-shaped AuNPs. De Jong and co-workers detected AuNPs, by inductively coupled plasma mass spectrometry in the blood, liver, spleen, lung, kidney, testis, thymus, heart and brain after intravenous injection of male rats with 10-, 50-, 100- and 250-nm spherical AuNPs [122]. The highest amount of Au was

detected in the blood, liver and spleen with lower amounts in the lungs, kidneys, testis, thymus, heart and brain, 24 h post injection. AuNPs of 10-nm were the most widespread through different organs, with the highest Au content in the liver, followed by the spleen (i.e., organs of the **mononuclear phagocyte system** [MPS] or, formerly, RES). After 24 h, the percent of injected dose of Au (g^{-1} tissue) was found to be 46, 21, 44, and 31% in the liver for 10, 50, 100 and 250 nm AuNPs, respectively, and in the spleen, these percentages were 2.2, 1.3, 1.4 and 1.2%, respectively. When AuNPs are functionalized with PEG, different trends are observed [123]. After tail vein injection of white rats, the accumulation of Au in the liver and spleen appears to decrease with decreasing nanoparticle size from 50 to 15 nm. Conversely, the blood showed the greatest amount of Au after 24 h when 15-nm PEG–AuNPs were administered. Having a higher concentration in the blood, the 15-nm nanoparticles have a greater probability of recirculating and accumulating into RES organs, as well as inflamed and/or malignant disease sites.

It is apparent from the abovementioned trends that a systematic examination of pharmacokinetic and biodistribution parameters for different nanoparticle sizes and surface chemistries must be done. Perrault *et al.* have performed a thorough examination of blood pharmacokinetics as well as tumor accumulation of AuNPs 25–119 nm in HD, coated with different molecular weights of PEG [124]. PEG was chosen as the surface coating for AuNPs as it can reduce MPS uptake and clearance. Decreasing nanoparticle size and increasing the molecular weight of the PEG coating increases the blood half-life, as demonstrated after intravenous injection in CD1 mice. The trend is better displayed by particle set A (Figure 4A). Passive tumor targeting, utilizing the EPR effect, was also examined in athymic nude CD1 mice bearing subcutaneous MDA-MB-435 xenograft tumors after intravenous injections of the PEG-coated AuNPs from particle set B (Figure 4A). The blood half-lives were similar to those observed in the non-tumor-bearing mice. Although nanoparticle accumulation in the tumor is the target of this work, determining nanoparticle uptake by MPS organs is important since any accumulation there will compete with nanoparticle accumulation at the tumor site. For all nanoparticle sizes, accumulation in the liver and spleen increased over time with greater apparent filtering capacity exhibited by the spleen (% initial dose [ID] g^{-1} tissue). Cumulative tumor accumulation was found to be greatest for 61 nm HD PEGylated (5 kDa) AuNPs with trends following: 61>83>99>40>22 nm HD. Size-dependent permeation of the tumor interstitium was also evaluated after 8-h circulation of PEGylated nanoparticles, revealing decreasing permeation with increasing nanoparticle size. 61-nm HD PEGylated AuNPs (~32–45 nm core diameter with 5 kDa PEG) exhibited optimal blood half-life and tumor accumulation profiles with tumor accumulation, MPS biodistribution and blood half-life comparable for increasing PEG molecular weight. Due to their less optimal intratumoral penetration characteristics, administration of a combination of 61-nm HD PEGylated AuNPs and sizes below may be well suited for future therapeutic applications. Oh and co-workers have additionally investigated size-dependent cellular uptake of cell-penetrating peptide functionalized AuNPs, 2.4–89 nm in diameter, *in vitro* [125]. Particles were conjugated to PEG dithiolate-linked with the protein transduction domain of the HIV-Tat peptide and uptake was visually assessed in COS-1 monkey kidney cells. Surprisingly, particles >16 nm (electron microscopic diameter) exhibited negligible uptake while 5.5–8.2 nm AuNPs exhibited predominant perinuclear and membrane localization. Nanoparticles of size 2.4 nm, additionally exhibited nuclear localization.

The biodistribution profiles of rod-shaped AuNPs is also of current interest as these structures have shown potential in drug- and/or gene-delivery applications [126–129] and PTT [8,9,45–48,73,84]. Systemically administered, AuNPs (55×13 nm) with no polymer functionalization have exhibited sustained circulation in the blood of Sprague-Dawley rats over periods as long as 14 days [130]. Accumulation in RES organs was observed with a

plateau in AuNP accumulation in the liver at 1 day circulation. Retention in the liver over 28 days was also found, suggesting diminished capacity for hepatobiliary clearance/excretion of CTAB-capped AuNPs. Splenic accumulation exhibited a gradual increase over this time period, with lung, kidney, heart, brain, bone and muscle accumulation likewise decreasing. CTAB-AuNPs were observed by transmission electron microscopy (TEM) in the lysosomes of both the spleen and liver, owing to the digestive nature of the acidic lysosome environment present in Kupffer cells of the liver and lymphocytes of the spleen. Fecal excretion suggested some capacity for hepatobiliary excretion of these size AuNPs; however, due to their lack of adequate polymer stabilization, these results may not reflect those observable with PEGylated AuNPs. Much like the spherical AuNPs, PEGylation of AuNPs can mitigate RES/MPS organ uptake [131]. Upon coating 65×11 nm AuNPs with PEG, Niidome *et al.* observed no accumulation in major organs, with the exception of the liver, 72 h post injection. Here, PEGylation imparted dramatic improvements to both the pharmacokinetics and biodistribution profiles of systemically administered AuNPs. Von Maltzahn and co-workers found that PEGylated AuNPs (5 kDa PEG-SH) can exhibit up to 17 h blood half-life in nude mice with approximately 7% ID tumor accumulation after 72 h [47]. El-Sayed and co-workers found that the blood half-life of PEGylated AuNPs is reduced by 25–48% when co-conjugated with active targeting ligands and that subsequent tumor accumulation is altered by −57 to +67% in nude mice (24 h, relative to fully PEGylated nanorods) [132]. Systemically administered PEGylated AuNPs have exhibited sustained RES organ accumulation over a 28-day period with liver accumulation decreasing from approximately 72–63% ID and splenic accumulation decreasing approximately 8–7% ID over this period. Like other nanoparticles, the blood half-life of PEGylated AuNPs generally increases with PEG grafting density [121] and/or PEG molecular weight, both of which can augment subsequent passive tumor accumulation.

Given their utility in drug delivery, one might reasonably question whether Au nanospheres or nanorods are preferable for biomedical targeting/delivery. Although rod-shaped nanoparticles exhibit greater *in vivo* transvascular flux relative to spherical particles of equivalent HD [133], these particles also exhibit diminished cellular uptake *in vitro* [133]. Chauhan *et al.* have examined the transmembrane permeability, gel diffusivity and transvascular flux of PEGylated semiconductor nanoparticles and nanorods of 33–35 nm HD. They found that in all cases, nanorods exhibited optimal transport properties and 4.1-times more rapid transvascular penetration, the latter likely due to reduced steric hindrance from and viscous drag near vessel pore walls. Notwithstanding, Chithrani and co-workers found that Au nanospheres (14 and 74 nm diameter by TEM) exhibit higher intracellular accumulation in HeLa cervical carcinoma cells than either 14×40 or 14×74 nm AuNPs, with 50-nm spheres exhibiting the highest accumulation among a range of sizes/shapes. Readers may note, however, that direct comparison between Au nanospheres and nanorods can be difficult given the surface ligands present during their synthesis and the extent to which they can be exchanged to match one another's physiochemical properties.

Targeting approaches for biomedical AuNPs

Passive targeting, active targeting, or a combination of both strategies can be used to achieve tumor-specific particle accumulation and drug delivery. Passive targeting utilizes the EPR effect, characteristic of many diseased sites [134]. Active targeting can be achieved by conjugating AuNPs with various tumor-targeting agents, such as antibodies, peptides, and small molecules such as folic acid.

Efficient accumulation of AuNPs in diseased cells, organs and tumors is necessary to achieve optimal drug delivery. With passive targeting being important for the accumulation of AuNPs at diseased sites, Chithrani *et al.* studied the size and shape dependent targeting of

spherical AuNPs and AuNPs to HeLa cells [135]. Inductively coupled plasma atomic emission spectroscopy was used to determine the Au content in cells after incubation with nanoparticles. Cellular uptake kinetics showed that 50 nm citrate-capped spherical AuNPs exhibited optimal (per particle) uptake relative to 14, 30, 74 and 100 nm citrate-AuNPs (50>30>14>74>100 nm core diameter). Uptake half-lives of 14, 50, and 74 nm AuNPs were 2.10, 1.90, and 2.24 h, respectively. When these nanoparticles were coated with a serum protein known to enter cells via transferrin receptor-mediated endocytosis (transferrin), uptake decreased. Prior to transferrin modification of the AuNPs, the overall charge on the nanoparticle surface is negative due to the adsorbed citric acid groups, which would be expected to display decreased uptake into HeLa cells caused by electrostatic repulsion with the negatively charged cell surface. Therefore, it is possible that the citric acid groups desorb or are charge (Debye) screened from the surface of the nanoparticle by nonspecific adsorption of serum proteins, as suggested by infrared vibrational analysis, which showed high concentrations of primary and secondary amines on the nanoparticle surface, which would allow for uptake to take place unimpeded by charge–charge repulsion. Uptake was found to be not only dependent on AuNP size and surface chemistry, but also shape. Spherical citrate–AuNPs with core diameters of 74 and 14 nm showed greater per particle uptake in HeLa cells than 74×14-nm citrate/CTAB-AuNPs, by 500 and 375%, respectively. The ratio of nanoparticle length to width also affected the uptake, such that 40×14-nm nanorods display a greater uptake in HeLa cells than 74×14-nm particles. This result may arise from the fact that the long axis of the AuNP could essentially take up more receptors on the cell surface than the smaller nanorods or spherical AuNPs, thereby reducing availability of receptors to other nanoparticles.

El-Sayed and co-workers have demonstrated the specific targeting of cancer cells (HSC and HOC cell lines) with anti-EGFR-conjugated AuNPs via dark-field light scattering microscopy [136–139]. Due to overexpression of EGFR on the surface of cancer cells, the preferential binding of these nanoparticles to cancer cell surfaces was observed (Figure 5B & C) relative to noncancerous HaCaT cells (Figure 5A).

Peptide conjugation is another method by which active, site-specific targeting of cancer may be realized for enhanced drug delivery. Chanda *et al.* recently utilized bombesin peptide (BBN)-functionalized AuNPs to target the gastrin-releasing peptide (GRP) receptor with high affinity. GRP is overexpressed particularly in prostate, breast and small-lung carcinoma [140]. BBN–AuNPs were administered intraperitoneally into prostate tumor-bearing severe combined immunodeficiency mice to minimize particle uptake by liver Kupffer cells. BBN–AuNPs exhibited GRP-enhanced tumor accumulation and decreased uptake in the liver, as compared with radiotracer-labeled BBN and nonspecific protein-conjugated AuNPs. BBN functionalization of AuNPs, thus, not only enhanced site-specific targeting of prostate tumor cells, but also minimized RES uptake.

Dixit *et al.* developed a folate receptor-targeted AuNP by attaching PEG to the AuNP surface via the disulfide moiety of thioctic acid and cross-coupling with folic acid [141]. Folic acid receptor (FR) is upregulated in many cancers, with the FR density increasing with the stage/grade of cancer. After malignant transformation, FR becomes accessible in blood circulation. Because FR has a high affinity for folic acid (K_d ~0.1 nM), folic acid conjugation can result in high uptake via receptor-mediated endocytosis. AuNPs, 10 nm in core diameter, were chosen due to their ability to passively target via the EPR effect. After 1 and 2 h incubation of FR-positive KB tumor cells with folic acid–AuNPs, TEM images showed that 20% of the cells contained a large number of nanoparticles, whereas the PEG–AuNPs appeared only at the periphery of the cells. To demonstrate the specificity of the folic acid–AuNPs, incubation with WI-38 cells (FR-negative) showed minimal nanoparticle uptake. The folate receptor-targeting competitive inhibitor, methotrexate, has also been

conjugated to AuNPs and used for folate receptor targeting and enhanced methotrexate drug efficacy *in vitro* [142].

Hormone receptors are tremendously important in the growth and progression of malignancies such as breast and prostate cancer. A total of 80–90% of breast cancers express estrogen receptor (ER)[143] and 60–70% of prostate cancers express androgen receptor [144]. Classically, these proteins function as intracellular gene transcription factors; however, a significant portion of these and other hormone receptors are now known to be plasma membrane associated [145] and participate in a range of nongenomic cellular actions following post-translational palmitoylation and caveolin-1 association [146,147]. Because these membrane-bound receptors maintain binding affinity for their endogenous hormones, antibodies of their intracellular receptors and antagonist ligands[145,147,148], we and others have recently proposed that membrane-localized hormone receptors may be viable cell-surface targets for tissue-selective drug delivery of multifunctional nanoparticle conjugates to breast and prostate cancers. Such strategies also provide opportunities for the use of currently employed small-molecule hormone receptor antagonist chemotherapeutics as combined targeting and therapeutic ligands for the targeted diagnosis and treatment of these diseases. To this end, we have developed platforms for the selective delivery of multifunctional AuNPs (~50 nm in HD) to breast and prostate cancers using polymer-stabilized AuNPs. Anti-estrogen chemotherapeutic molecules were appended with thiolated PEG at positions that minimally interfere with receptor binding, thus allowing nanoparticle anchoring via Au–S bond formation. Anti-estrogen AuNPs were conjugated with a derivative of the breast cancer chemotherapeutic tamoxifen. Optical dark-field light scattering microscopy showed that our antiestrogen nanoparticles were selectively delivered to ER-positive MCF-7 breast cancer cell in a receptor- and ligand-dependent manner. Time-dependent dose–response cytotoxicity studies found that the nanoparticle conjugates were more than four orders of magnitude more potent than their free drugs ligands, and that drug molecule potency was enhanced two-to-three-fold compared with an equivalent concentration of nanoparticle ligands. We observed no toxicity at therapeutically relevant concentrations following endocytotic suppression (4°C), nor did we observe toxicity to ER-negative breast cancer cells (MDA-MB-231). Anti-estrogen nanoparticles also competitively engaged ER, demonstrating concentration-dependent suppression of uptake by estradiol administration and near complete abrogation of cytotoxicity. *In vitro* laser PTT also showed power-dependent cytotoxicity to breast cancer cells incubated with pM carrier concentrations (24 h).

Targeting hepatocytes is important in drug-delivery treatments of liver cancer and in order to improve the challenges faced with this type of drug delivery, Bergen *et al.* conjugated AuNPs with PEG and a monovalent galactose-targeting ligand (gal) specific to the asialoglycoprotein receptor [149]. Using a mouse model, they tested the dependence of AuNP size (50–150 nm HD, based on the 200 nm effective size limit for liver sinusoisal fenestrations), surface charge, surface hydrophilicity and ligand density on hepatocyte targeting. Hepatocytes were separated from the liver and, after only 20 min, 25% of the gal–PEG-conjugated AuNPs had accumulated in the liver, while only 2% of the PEG-conjugated nanoparticles were taken up by the liver. The 50-nm gal–PEG conjugated nanoparticles were found to be best for hepatocyte targeting, exhibiting a 2.5-fold increase of Au in hepatocytes compared with the 80-, 100- and 150-nm gal–PEG conjugated AuNPs and nonspecific PEG-conjugated AuNPs. These studies suggest that the AuNP can also be exploited as a vector for specific nonviral gene delivery to hepatocytes in the future.

Enhanced drug delivery & efficacy of AuNP conjugates

As stated earlier, the large surface area to volume ratio of AuNPs allow for high drug and/or prodrug loading capacities, which can significantly lower the minimum effective dosages relative to free drug molecules. Recently, several groups have focused on enhancing the cytotoxicity of current chemotherapeutic drugs through AuNP coupling. El-Sayed and co-workers utilized AuNPs conjugated to thiol-PEGylated tamoxifen derivatives to selectively target breast cancer cells that overexpress the ER [38]. The PEG linker allowed for increased particle stability in the cell culture media as well as reduced the nonspecific binding of serum proteins to the surface of the conjugated particle. Increased potency of doxorubicin hydrochloride (DOX) has been reported after its conjugation to natural gum reduced/stabilized AuNPs [150]. DOX, a member of the anthracycline ring class of antibiotics, is one of the most prominent chemotherapeutic drugs and is used for the treatment of a variety of cancers. Although this drug is commonly used, it is limited by its extremely unfavorable side effects and is, therefore, not approved for the treatment of certain cancers, such as brain cancer. Dhar *et al.* demonstrated that through the conjugation with AuNPs, a large increase in DOX toxicity was achieved [150]. Reduced cell viability was attributed to the efficient endocytotic uptake of DOX-conjugated AuNPs compared with the free DOX molecules, which must passively diffuse across the membrane. Their results suggest that DOX-coupled AuNPs could lower the effective dose administered to patients during treatment and aid in the transport of the drug across the blood–brain barrier. Similarly, there has been investigation into the cytotoxicity of oxaliplatin-conjugated AuNPs. Oxaliplatin is an analog of cisplatin and is readily used in colorectal cancer chemotherapy. Its mechanism of action is to intercalate into DNA and inhibit DNA synthesis in cancer cells. Although it is very effective, oxaliplatin does not specifically target cancer cells and, therefore, can attack other rapidly dividing healthy cells. In order to improve this form of chemotherapy, enhanced drug delivery must be achieved. Brown *et al.* demonstrated increased potency of oxaliplatin when conjugated to the surfaces of AuNPs through thiolated PEG linkers [151]. Their reported fivefold increase in *in vitro* cytotoxicity after conjugation was again attributed to the efficient uptake of the particle conjugates through endocytosis into cancer cells.

When introducing therapeutic agents in their 'free' form to a biological environment, their cellular uptake can be limited by several factors including solubility, *in vivo* stability and nonspecific biodistribution. Several groups have shown that coupling chemotherapeutic drugs to AuNPs helps improve the drug's solubility and uptake into cancerous tissues [54,55]. One treatment area that has the potential to greatly benefit from coupling to AuNPs is photodynamic therapy (PDT). PDT is a form of cancer treatment that utilizes light, photosensitizers and tissue oxygen [152]. Traditionally, photosensitizing agents such as porphyrins are intravenously injected and passively accumulate in diseased tissues. After photosensitizer accumulation, diseased tissues are excited by specific wavelengths of light, causing energy transfer from the photosensitizer to molecular oxygen in the surrounding tissue. This transfer of energy generates singlet oxygen, a reactive oxygen species that induces cell death through apoptosis. A common and significant drawback to this form of chemotherapy is the photosensitizer's lack of solubility in physiological environments, which inhibits its uptake/accumulation into the diseased tissues. In an effort to improve PDT, Burda and co-workers conjugated Pc4, a photosensitizer, to 5-nm AuNPs and studied the coupled particles' uptake and delivery (Figure 6A) [153]. Unlike free Pc4, the conjugated form was soluble in aqueous environments. Their experiments revealed that tumor-bearing mice that had been injected with Pc4–AuNPs showed increased delivery and accumulation efficiency at the tumor site after 2 h (Figure 6B). When only Pc4 was intravenously introduced, it took an average of 2 days to achieve maximum drug accumulation at the tumor site.

Platinum (IV) prodrug complexes also have the potential to benefit from the coupling to AuNPs. Cisplatin, the active analog of Pt(IV) prodrugs, is a first-line chemotherapeutic drug for a number of cancers including ovarian, cervical and testicular cancers. Although cisplatin is very effective as a cancer treatment, it has a number of major side effects such as kidney toxicity (nephrotoxicity) and irreversible nerve damage (neuropathy) [154,155]. In order to combat these drawbacks, Lippard and co-workers utilized a Pt(IV) prodrug compound tethered to an amine-functionalized DNA AuNP conjugate [40]. The Pt(IV) compound was only activated into its cytotoxic cisplain form, Pt(II), after crossing the cell membrane and undergoing intracellular reduction. Their experiments showed a significant increase in cytotoxic effects for the Pt(IV)–AuNP complex when compared with the free Pt(IV) prodrug, as well as the (free) active form of the drug, cisplatin. Their results demonstrated the capability of AuNPs to be used as drug-delivery vehicles in order to improve a drug's uptake and cytotoxic effects, while simultaneously providing potential therapeutic and diagnostic imaging enhancement (*vide infra*).

AuNPs as photoactivatable prodrugs

In addition to facile surface modification and their large surface-to-volume ratio, AuNPs also possess a number of other properties that can be employed in drug delivery applications. AuNP size/shape can be altered, affording the ability to tune their energy absorption profiles for use in PTT of solid tumors [8,9,45–48,64,84]. PTT typically uses laser exposure in the NIR (i.e., 650–900 nm) region, to induce cytotoxic damage in diseased tissues through the selective administration of heat sufficient to induce hyperthermic cellular responses [45,87–90]. NIR light is chosen for this form of therapy due to minimal absorption by tissues and physiological fluids at these wavelengths [85]. AuNPs such as nanorods, nanoshells and nanocages, which have maximum absorption in the NIR, are optimal for this treatment method because they have the ability to absorb NIR light and release the absorbed energy as heat at their localized accumulation site. Lin and co-workers carried out the first demonstration of AuNP PTT in 2003 [156]. They used 30-nm Au nanospheres that were conjugated with IgG antibodies to specifically target CD8 receptors on lymphocyte cells. After *in vitro* exposure to a nanosecond pulsed laser, 95% of cells that were treated with the Au nanospheres were killed.

Later, our group showed that AuNPs, with a maximum absorption at approximately 785 nm, could also be used as PTT agents to effectively kill cancer cells while leaving healthy cells unharmed [157]. AuNPs conjugated with antibodies to epidermal growth factor receptor (anti-EGFR) were specifically targeted to human oral squamous cell carcinoma cells, which are known to overexpress EGFR on their cell surface. Cancerous cells, which were labeled with the conjugated AuNPs, showed cell death at half the minimum laser energy needed to kill comparably treated healthy cells (Figure 7). Increased cell death at lower energies was attributed to the increased labeling of the malignant cells, which caused a greater local temperature increase and subsequent membrane disruption. Our group then expanded upon this work further in 2008 by introducing AuNPs that had been functionalized with PEG to nude mice by intravenous or interstitial injection [45]. PEGylated AuNPs showed tumor-site accumulation and enhanced absorption in the NIR region after administration. Furthermore, after exposure to a single continuous wave NIR laser, tumors that displayed AuNP accumulation exhibited dramatic inhibition in tumor growth with minimal damage to surrounding tissues. More than 50% of mice treated using our optimized treatment protocol showed no detectable disease at 2 weeks following a single administration of PEGylated AuNPs and a single 10-min laser exposure (Figure 1B). One notable advantage for the use of PEGylated Au nanotechnologies in the clinic is their classification by the FDA as a 'medical device' in PTT applications, allowing for substantially accelerated and less-costly approval processes. Human pilot studies exploring the use of intravenously administered

PEGylated silica–Au core–shell nanoparticles for NIR laser photothermal ablation of recurrent and/or refractory head and neck tumors are currently ongoing in the USA (NCT00848042; Nanospectra Biosciences, Inc.), with ongoing human pilot studies investigating the use of this technology for the treatment of primary prostate cancer in Mexico. Both studies are scheduled to be completed in the middle of this year.

Recently, Van de Broek *et al.* demonstrated that so-called 'branched AuNPs' functionalized with nanobodies also have the capability to be used in PTT [158]. Nanobodies are the smallest known fully functional antigen-binding fragments that were evolved from the variable domain of a camel heavy-chain-only antibody. The conjugated nanobodies have the ability to bind to HER2 antigen overexpressed on breast and ovarian cancer cells. In this work, nanobody-conjugated branched AuNPs were incubated with HER2-positive SKOV3 human ovarian carcinoma cells. After incubation, it was shown that the conjugated nanoparticles showed specific cell targeting when compared with control samples (Figure 8, top panel). Most importantly, after 5 min of laser exposure with a continuous wave laser (690 nm, 38 W/cm^2) malignant cells were efficiently killed (Figure 8, bottom panel). For further reading, those interested are directed to a review by Dreaden *et al.* for a more comprehensive discussion regarding various structures and approaches to PTT using Au nanotechnologies [9].

Evasion of multiple drug resistance

Multidrug resistance (MDR) – the ability of cancer cells to become resistant to distinct chemotherapeutic drugs of varying structure and functionality – has become a major obstacle for cancer drug delivery. MDR can be intrinsic in a specific cell line or can be acquired over time after repeated drug treatment [159]. One key player in MDR is P-glycoprotein, an efflux pump that recognizes and expels upwards of 50% of all chemotherapeutic drugs (e.g., anthracyclines, vinca alkaloids, taxanes, epidophyllotoxins, mitomycins and camptothecins) out of the plasma membrane [160], lowering cytoplasmic drug levels, increasing minimum-effective dosages and increasing off-target side effects. In an effort to combat this issue, researchers have turned to nanoscale drug carriers, due to the fact that nanoparticle coupling can augment drug transport and endosomally protect drugs from P-glycoprotein recognition. Cheng and co-workers coupled DOX, a DNA intercalater, to 5 nm PEGylated Au nanospheres through an intracellular enzyme-cleavable disulfide linkage [161]. To assess their conjugates' ability to overcome MDR, the intracellular uptake and cytotoxicity of the AuNP–drug conjugate was compared with the free drug in an MDR cell line, HepG2R. Their results showed that DOX-functionalized nanoparticles had an increased cellular uptake relative to that of free DOX, as well as an increased cytotoxicity towards the MDR cell line. The increased cytotoxicity observed with the conjugated Au nanospheres suggested that upon entry into the cell via endocytosis, the disulfide bond between the nanoparticle and the DOX molecule was cleaved by the combination of thiol-reducing enzymes and the acidic environment in the lysosomes. Wang *et al.* used a similar release strategy to investigate the ability of 30 nm AuNPs to deliver/release the DOX in MCF-7/ADR cells, a breast cancer drug-resistant cell line [162]. In this work, DOX was conjugated to Au nanospheres with a PEG spacer through an acid labile hydrazine linkage (Figure 9A). The group proposed that the Au nanospheres would increase intracellular DOX concentrations through endocytic uptake of the nanoparticles. Once inside the cell and acidic organelles (i.e., lysosomes), DOX would be released and become available to interfere with normal cellular processes (Figure 9B). To study the internalization and subsequent release of DOX from the nanoparticle, nanosurface energy transfer was utilized. Once attached to a AuNP, the fluorescence of DOX at 565 nm is quenched and was only restored after cleavage of the hydrazine linker in acidic environments. Using confocal microscopy and flow cytometry, they demonstrated that DOX conjugated AuNPs showed an increase in uptake

and release of the drug when compared with the free drug. Tetrazolium assays also revealed that the acid-responsive nanoparticles had increased cytotoxicity to the MCF-7 drug-resistant cell line when compared with the free drug and DOX–AuNPs that did not have the acid-responsive linker. This work suggests that AuNPs conjugated to chemotherapeutic drugs can overcome MDR through the increased particle uptake by endocytosis and the subsequent drug release.

Future perspective

While tremendous advances in the clinical translation of therapeutic Au nanotechnologies have been forged over the past decade, there remains a substantial body of work yet to be performed in order to realize broad acceptance of these platforms as first-line treatment modalities. One area of particularly pressing concern is the potential toxicity of these constructs and their unintended impacts on human health. In order to meet this urgent need, the National Institute of Standards and Technology, the FDA and the National Cancer Institute have established the Nanotechnology Characterization Laboratory to aid researchers in the regulatory review, preclinical testing/evaluation, and eventual translation of nanotechnologies intended for cancer therapies and diagnostics. While critically important in the short-term, clinical translation would also benefit from long-term studies investigating potential deleterious effects from chronic inflammation [163] associated with diminished clearance of these particle constructs, potential mutagenicity, and effects on reproductive health. Researchers in the field may also be better served to dispel many common misconceptions about AuNPs, such as their prohibitively high cost of production in large scale and our relative lack of exposure to these materials throughout much of the 20th century. As just two examples:

- The Au content present in a full-course dosage of TNFα–AuNPs recently administered in a Phase I clinical trial (NCT00356980; CytImmune Sciences, Inc.) [164] currently costs less than US 12¢ per patient and the quantity of Au salt used to produce the nanorods administered in our recent photothermal ablation studies [45] currently costs less than 23¢ per mouse [165].

- Recent studies indicate that nanoscale silverparticles can readily leach from larger Ag nanoparticles, and even bulk Ag in the form of decorative earrings, over the course of just weeks [166], suggesting that human exposure to noble metal nanoparticles may date as far back as the advent of modern currency

Areas of research, such as high-throughput Au nanoconjugate synthesis/screening, low-cost models to predict excretion and larger-scale *in vivo* characterization to allow direct side-by-side comparison of these constructs are currently underexplored and in great need. Going forward, the biggest challenge to systemically delivered Au nanotechnologies will be mass balance; that is, the demonstration of efficient clearance/excretion and accounting for the subsequent accumulation/excretion of every microgram of these drugs that are administered. Some areas of particular optimism include laser PTT for tumors in poorly accessible regions or those near vital organs/tissues (e.g., vocal cords and nerves), enhanced radiation therapy, isolated limb perfusion techniques and intraoperative ablation of tumor margins. Given these challenges, those in the field should be mindful that although therapeutic Au nanotechnologies may have advanced quite rapidly into the clinic, compared with liposomal and monoclonal antibody technologies (which took nearly 30 years from their first description as potential therapeutic agents to receive FDA approval), the field still has tremendous room for growth and further exploration of the new and exciting properties/functionality yet to be discovered and clinically applied.

Supplementary Material

Refer to Web version on PubMed Central for supplementary material.

Acknowledgments

Key Terms

Au nanoparticles	Au structures with dimensions between 1 and 100 nm, which can be surface functionalized with as many as 1.5×10^7 molecules per square micron. Sometimes, AuNPs can serve as photothermal, photoacoustic, computed tomography, optical coherence tomography, radiotherapy and surface-enhanced Raman scattering contrast agents. When directed to discrete intracellular locations (e.g., peptide-directed perinuclear localization), AuNPs can also exhibit selective cytotoxic effects on cancer cells.
Enhanced permeability and retention effect	Posits that high-molecular-weight (nanoscale) compounds will preferentially accumulate at the sites of solid tumors due to the characteristically disordered architecture of their blood vessels, the low diffusivity of these compounds preventing their diffusion away from the tumor interstitium and the characteristically diminished lymphatic drainage from tumor sites.
Avidity	The ability of a macromolecule (or nanoparticle) to simultaneously bind multiple, adjacent sites on a structure to afford it increasingly selective target binding over mono-functional counterparts.
Hyperthermia	An increase in physiological temperature of 3–6°C or more that can induce cellular damage to which malignant cells are increasingly susceptible and which can act synergistically with chemotherapy, radiotherapy and/or immunotherapy treatments. Implicated by Coffey and co-workers as a possible contributor to the so-called 'Lance Armstrong effect'.
Near-IR window	Tissue penetration by light is most efficient in the near-IR (650–900 nm) wavelength region due to minimal attenuation by tissues/physiological fluids such as water and hemoglobin. Optical/near-IR photoexcitation and imaging are most efficient at these wavelengths.
Photothermal therapy	Selective administration of photons (often from a laser) that can induce therapeutic temperature increases sufficient for hyperthermic physiological response. Plasmonic photothermal therapy uses nanoscale metal particles that exhibit surface Plasmon resonance to serve as contrast agents that convert light into heat with high efficiency.
Hydrodynamic diameter	The apparent diameter of a nanoparticle, which includes its core diameter and contributions from its outer hydration shell. Hydrodynamic diameter, rather than core diameter, largely dictates

	the ability of a circulating nanoparticle to extravasate into a tumor site or to be excreted in the urine. Hydrodynamic diameter of an anisotropic nanoparticle is approximately its orientationally averaged hydrodynamic diameter.
Poly(ethylene glycol)	The most common polymer used to sterically stabilize systemically administered Au nanoparticles and to shield them from full immunogenic responses and/or protein adsorption. PEGylation greatly increases blood circulation times.
Mononuclear phagocyte system	Part of the immune system that consists of the phagocytic cells, located in reticular connective tissue. Uptake by the mononuclear phagocyte system is one of the primary off-target pathways by which circulating nanoscale particles are removed from circulation. The reticuloendothelieal system is a less contemporary term for the mononuclear phagocyte system.

References

Papers of special note have been highlighted as:

▪ of interest

▪▪ of considerable interest

1. Knop K, Hoogenboom R, Fischer D, Schubert US. Poly(ethylene glycol) in drug delivery. pros and cons as well as potential alternatives. Angew. Chem. Int. Ed. Engl. 2010; 49(36):6288–6308. [PubMed: 20648499]

2. Peer D, Karp JM, Hong S, Farokhzad OC, Margalit R, Langer R. Nanocarriers as an emerging platform for cancer therapy. Nat. Nanotechnol. 2007; 2(12):751–760. [PubMed: 18654426] . ▪ Seminal review on the use of nanotechnologies in cancer therapy.

3. Davis ME, Chen Z, Shin DM. Nanoparticle therapeutics: an emerging treatment modality for cancer. Nat. Rev. Drug Discov. 2008; 7(9):771–782. [PubMed: 18758474] . ▪ Discusses the design and clinical applications of nanoscale cancer therapeutics.

4. Shi J, Votruba AR, Farokhzad OC, Langer R. Nanotechnology in drug delivery and tissue engineering: from discovery to applications. Nano Lett. 2010; 10(9):3223–3230. [PubMed: 20726522] . ▪▪ Historical and forward-looking perspective on the use of nanotechnologies in biomedicine.

5. Petros RA, Desimone JM. Strategies in the design of nanoparticles for therapeutic applications. Nat. Rev. Drug Discov. 2010; 9(8):615–627. [PubMed: 20616808] . ▪▪ Well-referenced recent review on the design and use of nanoscale therapeutics with some unique historical perspectives.

6. Kim BYS, Rutka JT, Chan WCW. Nanomedicine. N. Engl. J. Med. 2010; 363(25):2434–2443. [PubMed: 21158659] . ▪ Concise, recent review on the applications of various nanotechnologies for clinicians.

7. Jain RK, Stylianopoulos T. Delivering nanomedicine to solid tumors. Nat. Rev. Clin. Oncol. 2010; 7(11):653–664. [PubMed: 20838415] . ▪▪ Comprehensive account of tumor physiology/ angiogenesis and implications for nanomedicine cancer drug design/applications.

8. Dreaden EC, Mackey MA, Huang X, Kang B, El-Sayed MA. Beating cancer in multiple ways using nanogold. Chem. Soc. Rev. 2011; 40(7):3391–3404. [PubMed: 21629885] . ▪▪ Recent 'tutorial review' on the chemistry, physics, design and applications of Au nanotechnologies in cancer diagnostics and therapeutics.

9. Dreaden EC, Alkilany AM, Huang X, Murphy CJ, El-Sayed MA. The golden age: gold nanoparticles for biomedicine. Chem. Soc. Rev. 2012; 41:2740–2779. [PubMed: 22109657] . ▪▪ Comprehensive 'critical review' on the synthesis, design, properties and applications of Au nanotechnolgies in clinical/preclinical medicine and commercial applications.

10. Torchilin VP, Lukyanov AN. Peptide and protein drug delivery to and into tumors: challenges and solutions. Drug Discov. Today. 2003; 8(6):259–266. [PubMed: 12623240]

11. Bae Y, Kataoka K. Intelligent polymeric micelles from functional poly(ethylene glycol)-poly(amino acid) block copolymers. Adv. Drug Deliv. Rev. 2009; 61(10):768–784. [PubMed: 19422866]

12. Oerlemans C, Bult W, Bos M, Storm G, Nijsen JFW, Hennink WE. Polymeric Micelles in anticancer therapy: targeting, imaging and triggered release. Pharm. Res. 2010; 27(12):2569–2589. [PubMed: 20725771]

13. Lukyanov AN, Torchilin VP. Micelles from lipid derivatives of water-soluble polymers as delivery systems for poorly soluble drugs. Adv. Drug Deliv. Rev. 2004; 56(9):1273–1289. [PubMed: 15109769]

14. Zhang L, Chan JM, Gu FX, et al. Self-assembled lipid–polymer hybrid nanoparticles. a robust drug delivery platform. ACS Nano. 2008; 2(8):1696–1702. [PubMed: 19206374]

15. Torchilin VP. Recent advances with liposomes as pharmaceutical carriers. Nat. Rev. Drug Discov. 2005; 4(2):145–160. [PubMed: 15688077]

16. Kaasgaard T, Andresen TL. Liposomal cancer therapy: exploiting tumor characteristics. Expert Opin. Drug Deliv. 2010; 7(2):225–243. [PubMed: 20095944]

17. Astruc D, Boisselier E, Ornelas C. Dendrimers designed for functions: from physical, photophysical, and supramolecular properties to applications in sensing, catalysis, molecular electronics, photonics, and nanomedicine. Chem. Rev. 2010; 110(4):1857–1959. [PubMed: 20356105]

18. Medina SH, El-Sayed MEH. Dendrimers as carriers for delivery of chemotherapeutic agents. Chem. Rev. 2009; 109(7):3141–3157. [PubMed: 19534493]

19. Mintzer MA, Grinstaff MW. Biomedical applications of dendrimers: a tutorial. Chem. Soc. Rev. 2011; 40(1):173–190. [PubMed: 20877875]

20. Ghosh P, Han G, De M, Kim CK, Rotello VM. Gold nanoparticles in delivery applications. Adv. Drug Deliv. Rev. 2008; 60(11):1307–1315. [PubMed: 18555555] . ▪ Review on the potential uses of Au nanotechnologies in delivery applications wth particular emphasis on novel chemical functionality and assembly.

21. Giljohann DA, Seferos DS, Daniel WL, Massich MD, Patel PC, Mirkin CA. Gold nanoparticles for biology and medicine. Angew. Chem. Int. Ed. Engl. 2010; 49(19):3280–3294. [PubMed: 20401880] . ▪▪ Comprehensive review on the synthesis, design and use of Au nanoparticles in biomedicine with special emphasis on oligonucleotide functionalization/delivery.

22. Lal S, Clare SE, Halas NJ. Nanoshell-enabled photothermal cancer therapy: impending clinical impact. Acc. Chem. Res. 2008; 41(12):1842–1851. [PubMed: 19053240]

23. Jokerst JV, Gambhir SS. Molecular imaging with theranostic nanoparticles. Acc. Chem. Res. 2011; 44(10):1050–1060. [PubMed: 21919457]

24. Trewyn BG, Slowing II, Giri S, Chen H-T, Lin VSY. Synthesis and functionalization of a mesoporous silica nanoparticle based on the sol–gel process and applications in controlled release. Acc. Chem. Res. 2007; 40(9):846–853. [PubMed: 17645305]

25. Bonacchi S, Genovese D, Juris R, et al. Luminescent silica nanoparticles. extending the frontiers of brightness. Angew. Chem. Int. Ed. Engl. 2011; 50(18):4056–4066. [PubMed: 21442691]

26. Xie J, Huang J, Li X, Sun S, Chen X. Iron oxide nanoparticle platform for biomedical applications. Curr. Med. Chem. 2009; 16(10):1278–1294. [PubMed: 19355885]

27. Thakor AS, Jokerst J, Zavaleta C, Massoud TF, Gambhir SS. Gold nanoparticles: a revival in precious metal administration to patients. Nano Lett. 2011; 11(10):4029–4036. [PubMed: 21846107] . ▪▪ Clinical- and theranostics-based perspective on contemporary biomedical Au nanotechnologies.

28. Harris JM, Chess RB. Effect of pegylation on pharmaceuticals. Nat. Rev. Drug Discov. 2003; 2(3):214–221. [PubMed: 12612647]

29. Duncan R. Polymer conjugates as anticancer nanomedicines. Nat. Rev. Cancer. 2006; 6(9):688–701. [PubMed: 16900224]

30. Napier ME, Desimone JM. Nanoparticle drug delivery platform. Polym. Rev. 2007; 47(3):321–327.

31. Hammond PT. Form and function in multilayer assembly: new applications at the nanoscale. Adv. Mater. 2004; 16(15):1271–1293.

32. Aggarwal S. What's fueling the biotech engine-2008. Nat. Biotechnol. 2009; 27(11):987–993. [PubMed: 19898448]

33. Wang H, Huff TB, Zweifel DA, et al. *In vitro* and *in vivo* two-photon luminescence imaging of single gold nanorods. Proc. Natl Acad. Sci. USA. 2005; 102(44):15752–15756. [PubMed: 16239346]

34. Zavaleta CL, Smith BR, Walton I, et al. Multiplexed imaging of surface enhanced Raman scattering nanotags in living mice using noninvasive Raman spectroscopy. Proc. Natl Acad. Sci. USA. 2009; 106(32):13511–13516. [PubMed: 19666578]

35. Lu W, Huang Q, Geng KB, et al. Photoacoustic imaging of living mouse brain vasculature using hollow gold nanospheres. Biomaterials. 2010; 31(9):2617–2626. [PubMed: 20036000]

36. Kim D, Jeong YY, Jon S. A drug-loaded aptamer-gold nanoparticle bioconjugate for combined CT imaging and therapy of prostate cancer. ACS Nano. 2010; 4(7):3689–3696. [PubMed: 20550178]

37. Von Maltzahn G, Centrone A, Park JH, et al. SERS-coded gold nanorods as a multifunctional platform for densely multiplexed near-infrared imaging and photothermal heating. Adv. Mater. 2009; 21:1–6.

38. Dreaden EC, Mwakwari SC, Sodji QH, Oyelere AK, El-Sayed MA. Tamoxifen-poly(ethylene glycol)-thiol gold nanoparticle conjugates: enhanced potency and selective delivery for breast cancer treatment. Bioconjug. Chem. 2009; 20(12):2247–2253. [PubMed: 19919059]

39. Giljohann DA, Seferos DS, Prigodich AE, Patel PC, Mirkin CA. Gene regulation with polyvalent siRNA-nanoparticle conjugates. J. Am. Chem. Soc. 2009; 131(6):2072–2073. [PubMed: 19170493]

40. Dhar S, Daniel WL, Giljohann DA, Mirkin CA, Lippard SJ. Polyvalent oligonucleotide gold nanoparticle conjugates as delivery vehicles for platinum(IV) warheads. J. Am. Chem. Soc. 2009; 131(41):14652–14653. [PubMed: 19778015]

41. Hainfeld JF, Dilmanian FA, Zhong Z, Slatkin DN, Kalef-Ezra JA, Smilowitz HM. Gold nanoparticles enhance the radiation therapy of a murine squamous cell carcinoma. Phys. Med. Biol. 2010; 55(11):3045–3046. [PubMed: 20463371]

42. Chithrani DB, Jelveh S, Jalali F, et al. Gold nanoparticles as radiation sensitizers in cancer therapy. Radiat. Res. 2010; 173(6):719–728. [PubMed: 20518651]

43. Qian XM, Peng XH, Ansari DO, et al. *In vivo* tumor targeting and spectroscopic detection with surface-enhanced raman nanoparticle tags. Nat. Biotechnol. 2008; 26(1):83–90. [PubMed: 18157119]

44. Jung Y, Reif R, Zeng Y, Wang RK. Three-dimensional high-resolution imaging of gold nanorods uptake in sentinel lymph nodes. Nano Lett. 2011; 11(7):2938–2943. [PubMed: 21667930]

45. Dickerson EB, Dreaden EC, Huang X, et al. Gold nanorod assisted near-infrared plasmonic photothermal therapy (PPTT) of squamous cell carcinoma in mice. Cancer Lett. 2008; 269(1):57–66. [PubMed: 18541363]

46. Chen J, Glaus C, Laforest R, et al. Gold nanocages as photothermal transducers for cancer treatment. Small. 2010; 6(7):811–817. [PubMed: 20225187]

47. Von Maltzahn G, Park J-H, Agrawal A, et al. Computationally guided photothermal tumor therapy using long-circulating gold nanorod antennas. Cancer Res. 2009; 69(9):3892–3900. [PubMed: 19366797]

48. Hirsch LR, Stafford RJ, Bankson JA, et al. Nanoshell-mediated near-infrared thermal therapy of tumors under magnetic resonance guidance. Proc. Natl Acad. Sci. USA. 2003; 100(23):13549–13554. [PubMed: 14597719]

49. Yuan F, Dellian M, Fukumura D, et al. Vascular permeability in a human tumor xenograft. Molecular size dependence and cutoff size. Cancer Res. 1995; 55(17):3752–3756. [PubMed: 7641188]

50. Yuan F, Leunig M, Huang SK, Berk DA, Papahadjopoulos D, Jain RK. Mirovascular permeability and interstitial penetration of sterically stabilized (stealth) liposomes in a human tumor xenograft. Cancer Res. 1994; 54(13):3352–3356. [PubMed: 8012948]

51. Pluen A, Boucher Y, Ramanujan S, et al. Role of tumor–host interactions in interstitial diffusion of macromolecules. Cranial vs subcutaneous tumors. Proc. Natl Acad. Sci. USA. 2001; 98(8):4628–4633. [PubMed: 11274375]

52. Matsumura Y, Maeda H. A new concept for macromolecular therapeutics in cancer chemotherapy: mechanism of tumoritropic accumulation of proteins and the antitumor agent smancs. Cancer Res. 1986; 46(12):6387–6392. [PubMed: 2946403]

53. Maeda H. Tumor-selective delivery of macromolecular drugs via the EPR effect: background and future prospects. Bioconjug. Chem. 2010; 21(5):797–802. [PubMed: 20397686]

54. Kim CK, Ghosh P, Pagliuca C, Zhu Z-J, Menichetti S, Rotello VM. Entrapment of hydrophobic drugs in nanoparticle monolayers with efficient release into cancer cells. J. Am. Chem. Soc. 2009; 131(4):1360–1361. [PubMed: 19133720]

55. Zhang X-Q, Xu X, Lam R, Giljohann D, Ho D, Mirkin CA. Strategy for increasing drug solubility and efficacy through covalent attachment to polyvalent DNA–nanoparticle conjugates. ACS Nano. 2011; 5(9):6962–6970. [PubMed: 21812457]

56. Lee SK, Han MS, Asokan S, Tung CH. Effective gene silencing by multilayered siRNA-coated gold nanoparticles. Small. 2011; 7(3):364–370. [PubMed: 21294265]

57. Lu W, Zhang G, Zhang R, et al. Tumor site–specific silencing of NF-κB p65 by targeted hollow gold nanosphere–mediated photothermal transfection. Cancer Res. 2010; 70(8):3177–3188. [PubMed: 20388791]

58. Guo S, Huang Y, Jiang Q, et al. Enhanced gene delivery and siRNA silencing by gold nanoparticles coated with charge-reversal polyelectrolyte. ACS Nano. 2010; 4(9):5505–5511. [PubMed: 20707386]

59. Bard, AJ.; Faulkner, LR. Electrochemical Methods: Fundamentals and Applications. 2nd Edition. New York, NY, USA: John Wiley & Sons Inc.; 2001.

60. Torchilin VP, Rammohan R, Weissig V, Levchenko TS. TAT peptide on the surface of liposomes affords their efficient intracellular delivery even at low temperature and in the presence of metabolic inhibitors. Proc. Natl Acad. Sci. USA. 2001; 98(15):8786–8791. [PubMed: 11438707]

61. Park J, Mattessich T, Jay SM, Agawu A, Saltzman WM, Fahmy TM. Enhancement of surface ligand display on PLGA nanoparticles with amphiphilic ligand conjugates. J. Control. Release. 2011; 156(1):109–115. [PubMed: 21723893]

62. Tassa C, Duffner JL, Lewis TA, et al. Binding affinity and kinetic analysis of targeted small molecule-modified nanoparticles. Bioconjug. Chem. 2009; 21(1):14–19. [PubMed: 20028085]

63. Jiang W, Kim BYS, Rutka JT, Chan WCW. Nanoparticle-mediated cellular response is size-dependent. Nat. Nanotechnol. 2008; 3(3):145–150. [PubMed: 18654486]

64. Lu W, Xiong C, Zhang G, et al. Targeted photothermal ablation of murine melanomas with melanocyte-stimulating hormone analoge-conjugated hollow gold nanospheres. Clin. Cancer Res. 2009; 15(3):876–886. [PubMed: 19188158]

65. Gobin AM, Lee MH, Halas NJ, James WD, Drezek RA, West JL. Near-infrared resonant nanoshells for combined optical imaging and photothermal cancer therapy. Nano Lett. 2007; 7(7):1929–1934. [PubMed: 17550297]

66. Suneil J, Jonathan AC, Alan RH, et al. Cell-specific radiosensitization by gold nanoparticles at megavoltage radiation energies. Int. J. Radiat. Oncol. Biol. Phys. 2010; 79(2):531–539. [PubMed: 21095075]

67. Roa W, Zhang X, Guo L, et al. Gold nanoparticle sensitize radiotherapy of prostate cancer cells by regulation of the cell cycle. Nanotechnol. 2009; 20(37):375101.

68. Hainfeld JF, Slatkin DN, Smilowitz HM. The use of gold nanoparticles to enhance radiotherapy in mice. Phys. Med. Biol. 2004; 49:N309–N315. [PubMed: 15509078]

69. Tong L, He W, Zhang YS, Zheng W, Cheng JX. Visualizing systemic clearance and cellular level biodistribution of gold nanorods by intrinsic two-photon luminescence. Langmuir. 2009; 25(21):12454–12459. [PubMed: 19856987]

70. Park J, Estrada A, Sharp K, et al. Two-photon-induced photoluminescence imaging of tumors using near-infrared excited gold nanoshells. Opt. Express. 2008; 16(3):1590–1599. [PubMed: 18542237]

71. Durr NJ, Larson T, Smith DK, Korgel BA, Sokolov K, Ben-Yakar A. Two-photon luminescence imaging of cancer cells using molecularly targeted gold nanorods. Nano Lett. 2007; 7(4):941–945. [PubMed: 17335272]

72. Hainfeld JF, Slatkin DN, Focella TM, Smilowitz HM. Gold nanoparticles: a new x-ray contrast agent. Brit. J. Radiol. 2006; 79(939):248–253. [PubMed: 16498039]

73. Cai QY, Kim SH, Choi KS, et al. Colloidal gold nanoparticles as a blood-pool contrast agent for x-ray computed tomography in mice. Invest. Radiol. 2007; 42(12):797–806. [PubMed: 18007151]

74. Sun IC, Eun DK, Na JH, et al. Heparincoated gold nanoparticles for liver-specific CT imaging. Chem. Eur. J. 2009; 15(48):13341–13347. [PubMed: 19902441]

75. Kim D, Park S, Lee JH, Jeong YY, Jon S. Antibiofouling polymer-coated gold nanoparticles as a contrast agent for *in vivo* x-ray computed tomography imaging. J. Am. Chem. Soc. 2007; 129(24): 7661–7665. [PubMed: 17530850]

76. Galanzha EI, Shashkov EV, Kelly T, Kim JW, Yang L, Zharov VP. *In vivo* magnetic enrichment and multiplex photoacoustic detection of circulating tumour cells. Nat. Nanotechnol. 2009; 4(12): 855–860. [PubMed: 19915570]

77. Rodriguez-Lorenzo L, Krpetic Z, Barbosa S, et al. Intracellular mapping with SERS-encoded gold nanostars. Integr. Biol. 2011; 3(9):922–926.

78. Mohs AM, Mancini MC, Singhal S, et al. Hand-held spectroscopic device for *in vivo* and intraoperative tumor detection. Contrast enhancement, detection sensitivity, and tissue penetration. Anal. Chem. 2010; 82(21):9058–9065.

79. Kneipp J, Kneipp H, Wittig B, Kneipp K. One- and two-photon excited optical pH probing for cells using surface-enhanced raman and hyper-raman nanosensors. Nano Lett. 2007; 7(9):2819–2823. [PubMed: 17696561]

80. Kang B, Mackey MA, El-Sayed MA. Nuclear targeting of gold nanoparticles in cancer cells induces DNA damage, causing cytokinesis arrest and apoptosis. J. Am. Chem. Soc. 2010; 132(5): 1517–1519. [PubMed: 20085324]

81. Kelly KL, Coronado E, Zhao LL, Schatz GC. The optical properties of metal nanoparticles: the influence of size, shape, and dielectric environment. J. Phys. Chem. B. 2002; 107(3):668–677.

82. Greczynski G, Salaneck WR. Photoelectron spectroscopy of hybrid interfaces for light emitting diodes: Influence of the substrate work function. Appl. Phys. Lett. 2001; 79(19):3185–3187.

83. Hartland GV. Optical studies of dynamics in noble metal nanostructures. Chem. Rev. 2011; 111(6):3858–3887. [PubMed: 21434614]

84. Dreaden, EC.; El-Sayed, MA.; El-Sayed, IH. Nanotechnology and nanostructures applied to head and neck cancer. In:. In: Preedy, VR.; Srirajaskanthan, R., editors. Nanomedicine and Cancer. Enfield, UK: Science Publishers; 2011.

85. Weissleder R. A clearer vision for *in vivo* imaging. Nat. Biotechnol. 2001; 19(4):316–317. [PubMed: 11283581]

86. Ntziachristos V, Yodh AG, Schnall M, Chance B. Concurrent MRI and diffuse optical tomography of breast after indocyanine green enhancement. Proc. Natl Acad. Sci. USA. 2000; 97(6):2767–2772. [PubMed: 10706610]

87. Wust P, Hildebrandt B, Sreenivasa G, et al. Hyperthermia in combined treatment of cancer. Lancet Oncol. 2002; 3(8):487–497. [PubMed: 12147435]

88. Bert H, Peter W, Olaf A, et al. The cellular and molecular basis of hyperthermia. Clin. Rev. Oncol./Hematol. 2002; 43(1):33–56.

89. Huff TB, Tong L, Zhao Y, Hansen MN, Cheng JX, Wei A. Hyperthermic effects of gold nanorods on tumor cells. Nanomedicine (Lond.). 2007; 2(1):125–132. [PubMed: 17716198]

90. Kampinga HH. Cell biological effects of hyperthermia alone or combined with radiation or drugs: a short introduction to newcomers in the field. Int J Hyperther. 2006; 22(3):191–196.

91. Nel AE, Mädler L, Velegol D, et al. Understanding biophysicochemical interactions at the nano-bio interface. Nat. Mater. 2009; 8(7):543–557. [PubMed: 19525947]

92. Tarazona-Vasquez F, Balbuena PB. Complexation of the lowest generation poly(amidoamine)-NH_2 dendrimers with metal ions, metal atoms, and Cu(II) hydrates: an *ab initio* study. J. Phys. Chem. B. 2004; 108(41):15992–16001.

93. Turkevich J, Stevenson PC, Hillier J. A study of the nucleation and growth processes in the synthesis of colloidal gold. Discuss. Faraday Soc. 1951; (11):55–75.

94. Frens G. Controlled nucleation for the regulation of the particle size in monodisperse gold suspensions. Nature. 1973; 241(105):20–22.

95. Ulman A. Formation and structure of self-assembled monolayers. Chem. Rev. 1996; 96(4):1533–1554. [PubMed: 11848802]

96. Ostwald, W. Lehrbuch der Allgemeinen Chemie. Leipzig, Germany: Wilhelm Engelmann; 1896.

97. Polte JR, Ahner TT, Delissen F, et al. Mechanism of gold nanoparticle formation in the classical citrate synthesis method derived from coupled *in situ* XANES and SAXS evaluation. J. Am. Chem. Soc. 2010; 132(4):1296–1301. [PubMed: 20102229]

98. Ojea-Jimènez I, Bastús NG, Puntes V. Influence of the sequence of the reagents addition in the citrate-mediated synthesis of gold nanoparticles. J. Phys. Chem. C. 2011; 115(32):15752–15757.

99. Xia H, Bai S, Hartmann JR, Wang D. Synthesis of monodisperse quasi-spherical gold nanoparticles in water via silver(i)-assisted citrate reduction. Langmuir. 2009; 26(5):3585–3589. [PubMed: 19877698]

100. Rodríguez-González B, Mulvaney P, Liz-Marzán LM. An electrochemical model for gold colloid formation via citrate reduction. Z. Phys. Chem. 2007; 221(3):415–426.

101. Kimling J, Maier M, Okenve B, Kotaidis V, Ballot H, Plech A. Turkevich method for gold nanoparticle synthesis revisited. J. Phys. Chem. B. 2006; 110(32):15700–15707. [PubMed: 16898714]

102. Brust M, Walker M, Bethell D, Schiffrin DJ, Whyman R. Synthesis of thiol-derivatised gold nanoparticles in a two-phase liquid–liquid system. Chem. Commun. 1994; (7):801–802.

103. Holgate CS, Jackson P, Cowen PN, Bird CC. Immunogold-silver staining: new method of immunostaining with enhanced sensitivity. J. Histochem. Cytochem. 1983; 31(7):938–944. [PubMed: 6189883]

104. Hainfeld JF, Dilmanian FA, Slatkin DN, Smilowitz HM. Radiotherapy enhancement with gold nanoparticles. J. Pharm. Pharmacol. 2008; 60(8):977–985. [PubMed: 18644191]

105. Pan Y, Neuss S, Leifert A, et al. Size-dependent cytotoxicity of gold nanoparticles. Small. 2007; 3(11):1941–1949. [PubMed: 17963284]

106. Jana NR, Gearheart L, Murphy CJ. Wet chemical synthesis of high aspect ratio cylindrical gold nanorods. J. Phys. Chem. B. 2001; 105(19):4065–4067.

107. Nikoobakht B, El-Sayed MA. Preparation and growth mechanism of gold nanorods (nrs) using seed-mediated growth method. Chem. Mater. 2003; 15(10):1957–1962.

108. Pérez-Juste J, Liz-Marzán LM, Carnie S, Chan DYC, Mulvaney P. Electric-field-directed growth of gold nanorods in aqueous surfactant solutions. Adv. Funct. Mater. 2004; 14(6):571–579.

109. Murphy CJ, Thompson LB, Chernak DJ, et al. Gold nanorod crystal growth. From seed-mediated synthesis to nanoscale sculpting. Curr. Opin. Colloid Interface Sci. 2011; 16(2):128–134.

110. Ha TH, Koo HJ, Chung BH. Shape-controlled syntheses of gold nanoprisms and nanorods influenced by specific adsorption of halide ions. J. Phys. Chem. C. 2006; 111(3):1123–1130.

111. Mcintosh CM, Esposito EA, Boal AK, Simard JM, Martin CT, Rotello VM. Inhibition of DNA Transcription using cationic mixed monolayer protected gold clusters. J. Am. Chem. Soc. 2001; 123(31):7626–7629. [PubMed: 11480984]

112. Liu X, Dai Q, Austin L, et al. A One-step homogeneous immunoassay for cancer biomarker detection using gold nanoparticle probes coupled with dynamic light scattering. J. Am. Chem. Soc. 2008; 130(9):2780–2782. [PubMed: 18257576]

113. Torchilin VP, Rammohan R, Weissig V, Levchenko TS. TAT peptide on the surface of liposomes affords their efficient intracellular delivery even at low temperature and in the presence of metabolic inhibitors. Proc. Natl Acad. Sci. USA. 2001; 98(15):8786–8791. [PubMed: 11438707]

114. Park J, Mattessich T, Jay SM, Agawu A, Saltzman WM, Fahmy TM. Enhancement of surface ligand display on PLGA nanoparticles with amphiphilic ligand conjugates. J. Control. Release. 2011; 156(1):109–115. [PubMed: 21723893]

115. Phadtare S, Kumar A, Vinod VP, et al. Direct assembly of gold nanoparticle 'shells' on polyurethane microsphere 'cores' and their application as enzyme immobilization templates. Chem. Mater. 2003; 15(10):1944–1949.

116. Nuzzo RG, Zegarski BR, Dubois LH. Fundamental studies of the chemisorption of organosulfur compounds on gold(III). Implications for molecular self-assembly on gold surfaces. J. Am. Chem. Soc. 1987; 109(3):733–740.

117. Owens IDE, Peppas NA. Opsonization, biodistribution, and pharmacokinetics of polymeric nanoparticles. Int. J. Pharm. 2006; 307(1):93–102. [PubMed: 16303268]

118. Tong L, He W, Zhang Y, Zheng W, Cheng JX. Visualizing systemic clearance and cellular level biodistribution of gold nanorods by intrinsic two-photon luminescence. Langmuir. 2009; 25(21): 12454–12459. [PubMed: 19856987]

119. Paciotti GF, Kingston DGI, Tamarkin L. Colloidal gold nanoparticles: a novel nanoparticle platform for developing multifunctional tumor-targeted drug delivery vectors. Drug Dev. Res. 2006; 67(1):47–54.

120. Longmire M, Choyke PL, Kobayashi H. Clearance properties of nano-sized particles and molecules as imaging agents: considerations and caveats. Future Med. Nanomed. 2008; 3(5): 703–717.

121. Akiyama Y, Mori T, Katayama Y, Nidome T. The effects of PEG grafting level and injection dose on gold nanorod biodistribution in the tumor-bearing mice. J. Control. Release. 2009; 139(1):81–84. [PubMed: 19538994]

122. De Jong WH, Hagens WI, Krystek P, Burger MC, Sips AJ, Geertsma RE. Particle size-dependent organ distribution of gold nanoparticles after intravenous administration. Biomaterials. 2008; 29(12):1912–1919. [PubMed: 18242692]

123. Terentyuk GS, Maslyakova GN, Suleymanova LV, et al. Circulation and distribution of gold nanoparticles and induced alterations of tissue morphology at intravenous particle delivery. J. Biophotonics. 2009; 2(5):292–302. [PubMed: 19434616]

124. Perrault SD, Walkey C, Jennings T, Fischer HC, Chan WCW. Mediating tumor targeting efficiency of nanoparticles through design. Nano Lett. 2009; 9(5):1909–1915. [PubMed: 19344179]

125. Oh E, Delehanty JB, Sapsford KE, et al. Cellular uptake and fate of pegylated gold nanoparticles is dependent on both cell-penetration peptides and particle size. ACS Nano. 2011; 5(8):6434–6448. [PubMed: 21774456]

126. Salem AK, Searson PC, Leong KW. Multifunctional nanorods for gene delivery. Nat. Mater. 2003; 2(10):668–671. [PubMed: 12970757]

127. Chen CC, Lin YP, Wang CW, et al. DNA-gold nanorod conjugates for remote control of localized gene expression by near infrared irradiation. J. Am. Chem. Soc. 2006; 128(11):3709–3715. [PubMed: 16536544]

128. Park J-H, Von Maltzahn G, Ong LL, et al. Cooperative nanoparticles for tumor detection and photothermally triggered drug delivery. Adv. Mater. 2010; 22(8):880–885. [PubMed: 20217810]

129. Park J-H, Von Maltzahn G, Xu MJ, et al. Cooperative nanomaterial system to sensitize, target, and treat tumors. Proc. Natl Acad. Sci. USA. 2010; 107(3):981–986. [PubMed: 20080556]

130. Wang LM, Li YF, Zhou LJ, et al. Characterization of gold nanorods *in vivo* by integrated analytical techniques. their uptake, retention, and chemical forms. Anal. Bioanal. Chem. 2010; 396(3):1105–1114. [PubMed: 20016883]

131. Niidome T, Yamagata M, Okamoto Y, et al. PEG-modified gold nanorods with a stealth character for *in vivo* applications. J. Control. Release. 2006; 114(3):343–347. [PubMed: 16876898]

132. Huang X, Peng X, Wang Y, Shin DM, El-Sayed MA, Nie S. A reexamination of active and passive tumor targeting by using rod-shaped gold nanocrystals and covalently conjugated peptide ligands. ACS Nano. 2010; 4(10):5887–5896. [PubMed: 20863096]

133. Chauhan VP, Popovi Z, Chen O, et al. Fluorescent nanorods and nanospheres for real-time *in vivo* probing of nanoparticle shape-dependent tumor penetration. Angew. Chem. Int. Ed. Engl. 2011; 50(48):11417–11420. [PubMed: 22113800]

134. Maeda H, Wu J, Sawa T, Matsumura Y, Hori K. Tumor vascular permeability and the EPR effect in macromolecular therapeutics: a review. J. Control. Release. 2000; 65(1–2):271–284. [PubMed: 10699287]

135. Chithrani BD, Ghazani AA, Chan WCW. Determining the size and shape dependence of gold nanoparticle uptake into mammalian cells. Nano Lett. 2006; 6(4):662–668. [PubMed: 16608261]

136. El-Sayed IH, Huang XH, El-Sayed MA. Surface plasmon resonance scattering and absorption of anti-EGFR antibody conjugated gold nanoparticles in cancer diagnostics: applications in oral cancer. Nano Lett. 2005; 5(5):829–834. [PubMed: 15884879]

137. El-Sayed IH, Huang XH, El-Sayed MA. Selective laser photo-thermal therapy of epithelial carcinoma using anti-EGFR antibody conjugated gold nanoparticles. Cancer Lett. 2006; 239(1): 129–135. [PubMed: 16198049]

138. Huang XH, El-Sayed IH, Qian W, El-Sayed MA. Cancer cell imaging and photothermal therapy in the near-infrared region by using gold nanorods. J. Am. Chem. Soc. 2006; 128(6):2115–2120. [PubMed: 16464114]

139. Huang XH, Jain PK, El-Sayed IH, El-Sayed MA. Determination of the minimum temperature required for selective photothermal destruction of cancer cells with the use of immunotargeted gold nanoparticles. Photochem. Photobiol. 2006; 82(2):412–417. [PubMed: 16613493]

140. Chanda N, Kattumuri V, Shukla R, et al. Bombesin functionalized gold nanoparticles show *in vitro* and *in vivo* cancer receptor specificity. Proc. Natl Acad. Sci. USA. 2010; 107(19):8760–8765. [PubMed: 20410458]

141. Dixit V, Van Den Bossche J, Sherman DM, Thompson DH, Andres RP. Synthesis and grafting of thioctic acid-PEG-folate conjugates onto au nanoparticles for selective targeting of folate receptor-positive tumor cells. Bioconjug. Chem. 2006; 17(3):603–609. [PubMed: 16704197]

142. Chen YH, Tsai CY, Huang PY, et al. Methotrexate conjugated to gold nanoparticles inhibits tumor growth in a syngeneic lung tumor model. Mol. Pharma. 2007; 4(5):713–722.

143. Osborne CK. Tamoxifen in the treatment of breast cancer. N. Engl. J. Med. 1998; 339(22):1609–1618. [PubMed: 9828250]

144. Heinlein CA, Chang C. Androgen receptor in prostate cancer. Endocr. Rev. 2004; 25(2):276–308. [PubMed: 15082523]

145. Pietras RJ, Márquez-Garbán DC. Membrane-associated estrogen receptor signaling pathways in human cancers. Clin. Cancer Res. 2007; 13(16):4672–4676. [PubMed: 17699844]

146. Lu ML, Schneider MC, Zheng YX, Zhang XB, Richie JP. Caveolin-1 interacts with androgen receptor – a positive modulator of androgen receptor mediated transactivation. J. Biol. Chem. 2001; 276(16):13442–13451. [PubMed: 11278309]

147. Pedram A, Razandi M, Sainson RCA, Kim JK, Hughes CC, Levin ER. A conserved mechanism for steroid receptor translocation to the plasma membrane. J. Biol. Chem. 2007; 282(31):22278–22288. [PubMed: 17535799]

148. Whitaker HC, Hanrahan S, Totty N, et al. Androgen receptor is targeted to distinct subcellular compartments in response to different therapeutic antiandrogens. Clin. Cancer Res. 2004; 10(21): 7392–7401. [PubMed: 15534116]

149. Bergen JM, Von Recum HA, Goodman TT, Massey AP, Pun SH. Gold nanoparticles as a versatile platform for optimizing physicochemical parameters for targeted drug delivery. Macromol. Biosci. 2006; 6(7):506–516. [PubMed: 16921538]

150. Dhar S, Reddy EM, Shiras A, Pokharkar V, Prasad BLV. Natural gum reduced/stabilized gold nanoparticles for drug delivery formulations. Chem. Eur. J. 2008; 14(33):10244–10250. [PubMed: 18850613]

151. Brown SD, Nativo P, Smith J-A, et al. Gold nanoparticles for the improved anticancer drug delivery of the active component of oxaliplatin. J. Am. Chem. Soc. 2010; 132(13):4678–4684. [PubMed: 20225865]

152. Dolmans DEJ, Fukumura D, Jain RK. Photodynamic therapy for cancer. Nat. Rev. Cancer. 2003; 3(5):380–387. [PubMed: 12724736]

153. Cheng Y, C. Samia A, Meyers JD, Panagopoulos I, Fei B, Burda C. Highly efficient drug delivery with gold nanoparticle vectors for *in vivo* photodynamic therapy of cancer. J. Am. Chem. Soc. 2008; 130(32):10643–10647. [PubMed: 18642918]

154. Hartmann JT, Kollmannsberger C, Kanz L, Bokemeyer C. Platinum organ toxicity and possible prevention in patients with testicular cancer. Int. J. Cancer. 1999; 83(6):866–869. [PubMed: 10597214]

155. Thompson SW, Davis LE, Kornfeld M, Hilgers RD, Standefer JC. Cisplatin neuropathy. Clinical, electrophysiologic, morphologic, and toxicologic studies. Cancer. 1984; 54(7):1269–1275. [PubMed: 6088023]

156. Pitsillides CM, Joe EK, Wei X, Anderson RR, Lin CP. Selective cell targeting with light-absorbing microparticles and nanoparticles. Biophys. J. 2003; 84(6):4023–4032. [PubMed: 12770906]

157. El-Sayed IH, Huang X, El-Sayed MA. Selective laser photo-thermal therapy of epithelial carcinoma using anti-EGFR antibody conjugated gold nanoparticles. Cancer Lett. 2006; 239(1): 129–135. [PubMed: 16198049]

158. Van de Broek B, Devoogdt N, D'Hollander A, et al. Specific cell targeting with nanobody conjugated branched gold nanoparticles for photothermal therapy. ACS Nano. 2011; 5(6):4319–4328. [PubMed: 21609027]

159. Van Vlerken LE, Amiji MM. Multi-functional polymeric nanoparticles for tumour-targeted drug delivery. Expert Opin. Drug Del. 2006; 3(2):205–216.

160. Constantinides PP, Wasan KM. Lipid formulation strategies for enhancing intestinal transport and absorption of P-glycoprotein (P-gp) substrate drugs: *in vitro/in vivo* case studies. J. Pharm. Sci. 2007; 96(2):235–248. [PubMed: 17051593]

161. Gu Y-J, Cheng J, Man CW-Y, Wong W-T, Cheng SH. Gold-doxorubicin nanoconjugates for overcoming multidrug resistance. Nanomedicine. 2011; 8(2):204–211. [PubMed: 21704592]

162. Wang F, Wang Y-C, Dou S, Xiong M-H, Sun T-M, Wang J. Doxorubicin-tethered responsive gold nanoparticles facilitate intracellular drug delivery for overcoming multidrug resistance in cancer cells. ACS Nano. 2011; 5(5):3679–3692. [PubMed: 21462992]

163. Cho W-S, Cho M, Jeong J, et al. Acute toxicity and pharmacokinetics of 13 nm-sized PEG-coated gold nanoparticles. Toxicol. Appl. Pharmacol. 2009; 236(1):16–24. [PubMed: 19162059]

164. Libutti SK, Paciotti GF, Byrnes AA, et al. Phase I and pharmacokinetic studies of CYT-6091, a novel PEGylated colloidal gold-rhTNF nanomedicine. Clin. Cancer Res. 2010; 16(24):6139–6149. [PubMed: 20876255]

165. Glover RD, Miller JM, Hutchison JE. Generation of metal nanoparticles from silver and copper objects: nanoparticle dynamics on surfaces and potential sources of nanoparticles in the environment. ACS Nano. 2011; 5(11):8950–8957. [PubMed: 21985489]

166. Shimizu T, Teranishi T, Hasegawa S, Miyake M. Size evolution of alkanethiol-protected gold nanoparticles by heat treatment in the solid state. J. Phys. Chem. B. 2003; 107(12):2719–2724.

167. Sau TK, Murphy CJ. Seeded high yield synthesis of short au nanorods in aqueous solution. Langmuir. 2004; 20(15):6414–6420. [PubMed: 15248731]

168. Oldenburg SJ, Averitt RD, Westcott SL, Halas NJ. Nanoengineering of optical resonances. Chem. Phys. Lett. 1998; 288(2–4):243–247.

169. Chen J, Mclellan JM, Siekkinen A, Xiong Y, Li Z-Y, Xia Y. Facile synthesis of gold/silver nanocages with controllable pores on the surface. J. Am. Chem. Soc. 2006; 128(46):14776–14777. [PubMed: 17105266]

170. Li W, Cai X, Kim C, et al. Gold nanocages covered with thermally-responsive polymers for controlled release by high-intensity focused ultrasound. Nanoscale. 2011; 3(4):1724–1730. [PubMed: 21321760]

171. Lu J, Dreisinger DB, Cooper WC. Cobalt precipitation by reduction with sodium borohydride. Hydrometallurgy. 1997; 45(3):305–322.

Patent

201. Oyelere, AK.; El-Sayed, MA.; Dreaden, EC. US0077581A1. 2011. (Pending)

Executive summary

Synthesis & conjugation: unique properties & unique applications

- Au nanoparticles can be easily and cheaply synthesized in large scale for cancer drug delivery, photothermal and intrinsic pharmacodynamic therapeutic applications.

- A 50-nm diameter Au nanoparticle can be chemically functionalized with roughly 120,000 distinct molecules, often two-to-three orders of magnitude higher than the surface-loading capabilities of liposomes and poly(lactic-co-glycolic acid) nanoparticles, respectively.

- Molecular groups, which anchor to the Au surface, can be modified to allow externally controllable or intrinsically triggered tethering and/or release.

- One Au nanoparticle can scatter as much light as 500,000 of the brightest commercially available fluorescent molecules and 2000 of the brightest commercially available quantum dots.

- Contrary to popular misconception, the production and biomedical use of Au nanoparticles is fairly low cost. For example, the Au content delivered in a full-course dosage of TNFα–Au nanoparticles recently administered in a Phase I clinical trial (NCT00356980) currently costs less than US 12¢ per adult patient; the quantity of Au chloride used to produce the nanorods administered in our recent photothermal therapy studies currently costs less than 23¢ per mouse.

Pharmacokinetics/ biodistribution: tumor-specific accumulation

- Polymer-functionalized (PEGylated) Au nanoparticles can exhibit long circulation times (as much as 51 h blood half-life) and can evade off-target uptake and blood clearance associated with recognition by the immune system.

- Due to their relatively large size, these structures preferentially accumulate at solid tumors due to the enhanced permeability and retention effect.

- Au nanoparticles greater than 6–8 nm in effective hydrodynamic diameter are not efficiently excreted in the urine and those approximately 50–60 nm in hydrodynamic diameter often exhibit optimal cellular uptake and intratumoral accumulation.

- Blood half-life and tumor penetration typically scales inversely with Au nanoparticle size for those not cleared in the urine.

Targeting: molecular-specificity & chemically tailored interaction(s)

- The accumulation and intracellular delivery of therapeutic Au nanoparticles can be targeted by small molecules, peptides, proteins, nucleic acids (including aptamers) and antibodies (as well as their fragments).

- Binding affinity of an Au nanoparticle can be tuned by simply changing the density of ligands on its surfaces, meaning that nanoparticle formulation can be tailored to a particular cancer type, stage or biopsy sample immediately prior to treatment.

- ■ As these structures are comparable in size to the distances between cell-surface target receptors, they can afford increasingly selective uptake versus monofunctionalized molecules due to multivalent avidity.

Efficacy: value-added drug-delivery vehicles

- ■ Au nanoparticles are well suited for drug-delivery applications, but can additionally serve as contrast agents for photothermal tumor ablation therapy, photoacoustic tomography/cytometry, x-ray computed tomography, optical coherence tomography, radiotherapy and Raman diagnostic imaging.

- ■ These structures can impart solubility to hydrophobic chemotherapeutics for intravenous administration and can protect/deliver molecules such as nucleic acids which are susceptible to enzymatic degradation and exhibit poor intracellular penetration.

- ■ Phase I clinical trials found that PEGylated Au nanoparticles are well-tolerated in humans at therapeutically relevant dosages for TNFα.

- ■ Au nanoparticles can allow increasingly specific and accelerated drug delivery, which minimizes unintended side effects, increases tolerable dosages and overcomes insensitivity in many treatment-resistance cell lines.
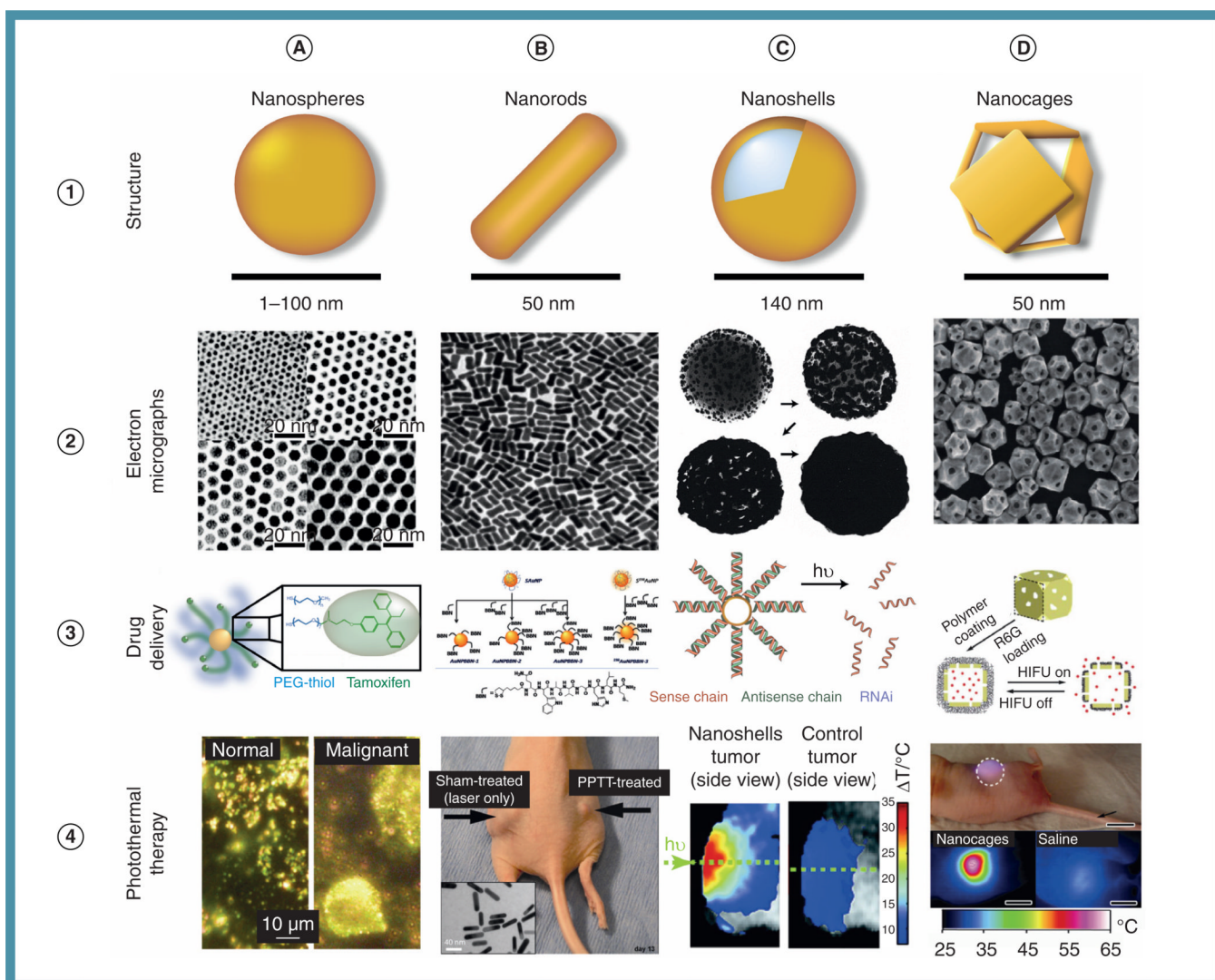
Figure 1. Applications of colloidal Au nanoparticles in drug delivery and laser photothermal therapy

(A) Au nanospheres; **(B)** Au nanorods, **(C)** Au nanoshell; and **(D)** Au nanocages.

HIFU: High-intensity focused ultrasound; PEG: Poly(ethylene glycol); PPTT: Plasmonic photothermal therapy; R6G: Rhodamine 6G.

(A2–A4) Reprinted with permission from [38,166,138]. © American Chemical Society (2009, 2003 and 2006), respectively.

(B2–B4) Reprinted with permission from [45]. © Elsevier (2008); [167] © American Chemical Society (2004); [140] © National Academy of Sciences (2010), respectively.

(C2;C4) Reprinted with permission from [48]. © National Academy of Sciences (2003); [168] © Elsevier (1998), respectively.

(D2–D4) Reprinted with permission from [46] © Wiley-VCH Verlag GmbH & Co. KGaA (2010); [169] © American Chemical Society (2006); [170] © Royal Society of Chemistry (2011), respectively.
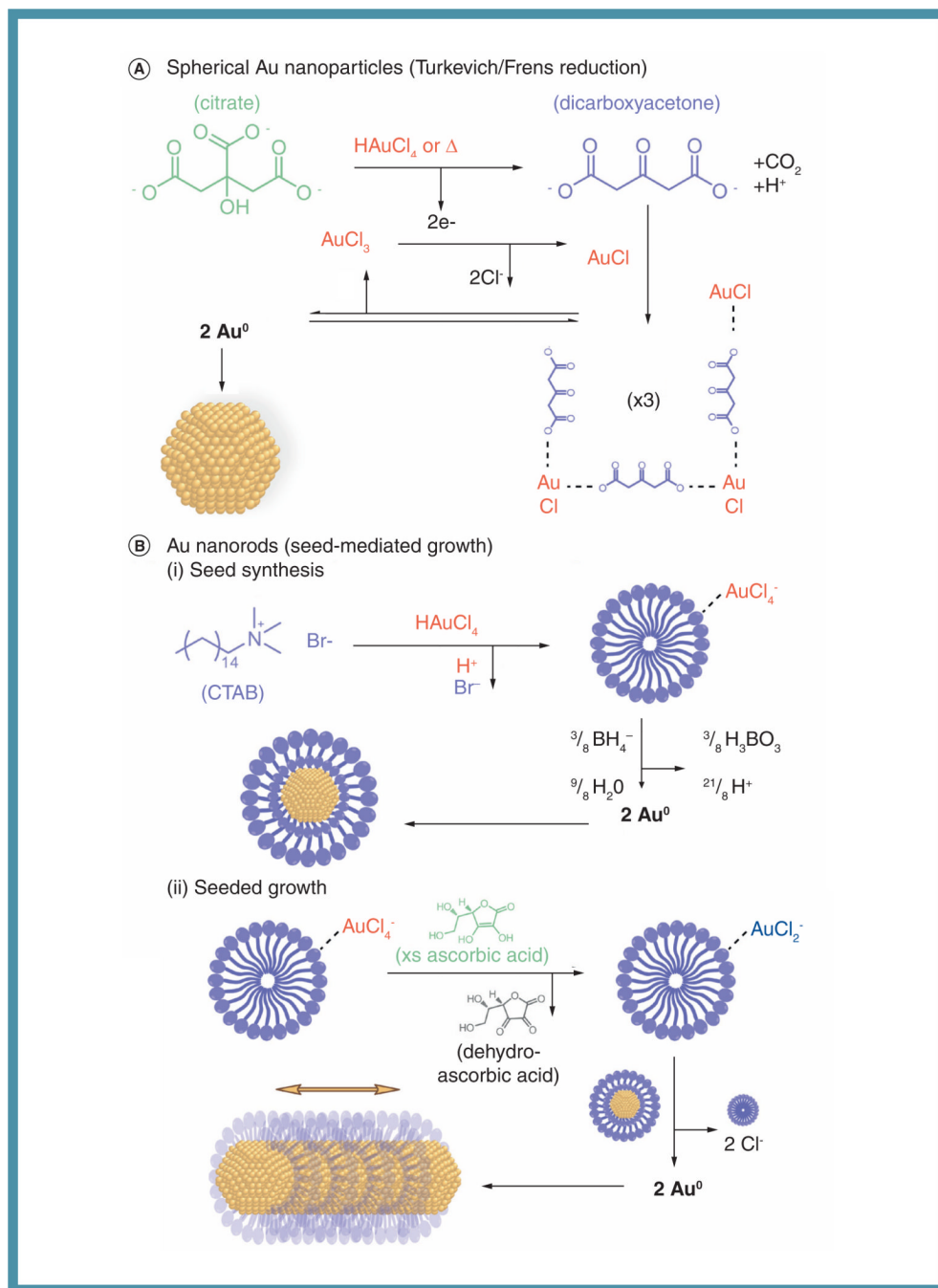
Figure 2. Turkevich/Frens synthesis of Au nanoparticles and seed-mediated growth of gold nanorods

(A) Au(III) is reduced to Au(I) when citrate is oxidized to dicarboxyacetone in the presence of chloroauric acid and/or heating. Au(I) chloride is believed to form a bidentate complex with dicarboxyacetone, which undergoes a disproportination reaction to form (2) zero-valent Au atoms and (1) Au(III) chloride. **(B)** (i) Au(III) chloride quantitatively displaces Br⁻ counterions in micelles of CTAB and subsequent borohydride reduction produces small (~1.5 nm diameter) seed nanoparticles surface stabilized by a CTAB-bilayer.(ii) Au(III) bound to CTAB micelles is reduced to Au(I) by ascorbic acid. Directional growth of Au nanorods occurs via crystallographically preferential reduction of Au(I) onto the seed

nanoparticles. For simplicity, note that **(B)** omits shape-directing contributions from adsorbed halide ions and Ag(I) ions.

CTAB: Cetyltrimethylammonium bromide.

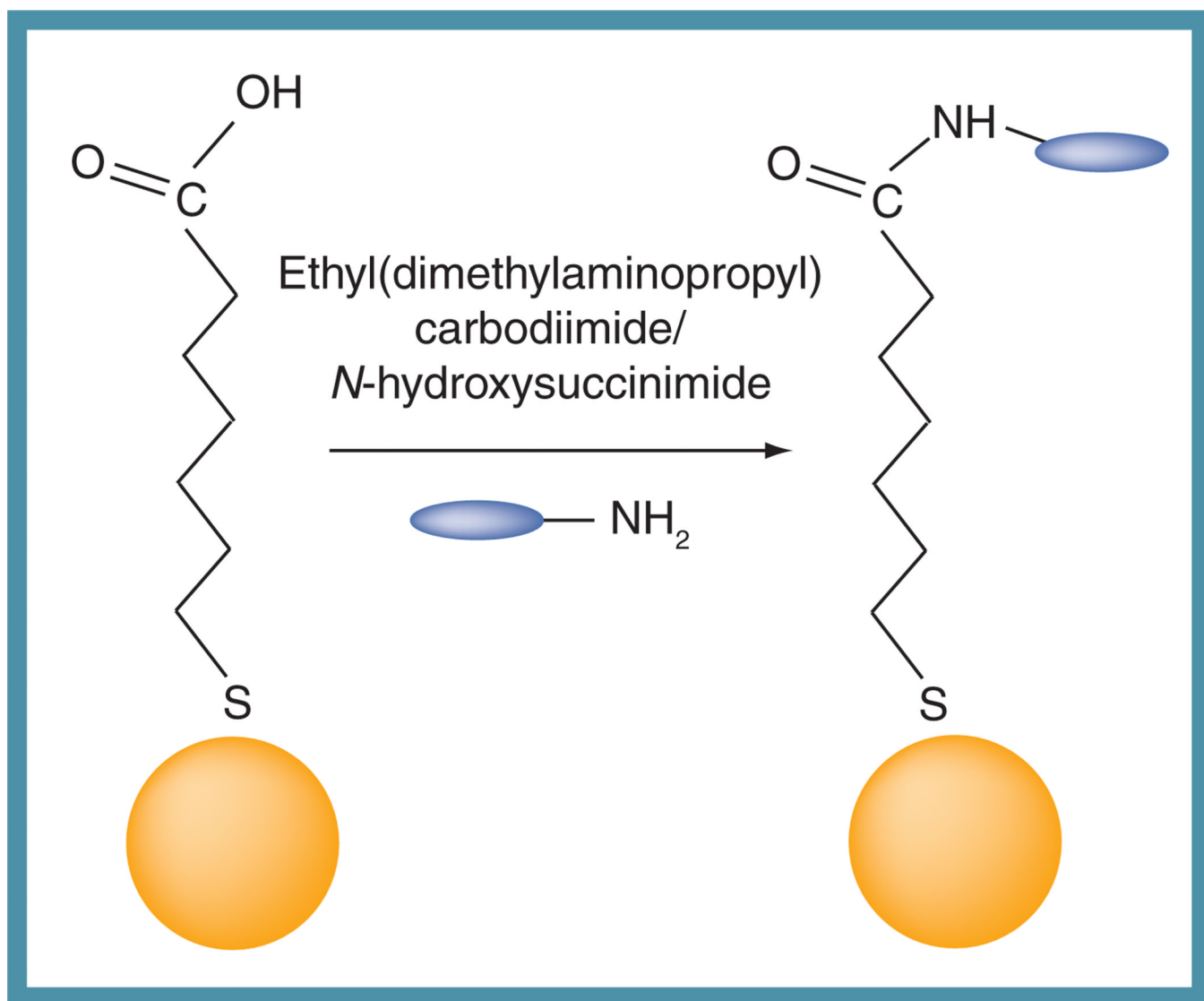(A) Data from [98,99].

(B) Data from [108,109,171].

Figure 3. Reaction of ethyl(dimethylaminopropyl) carbodiimide/*N*-hydroxysuccinimide coupling commonly used to conjugate various molecules to surface-functionalized Au nanoparticles.
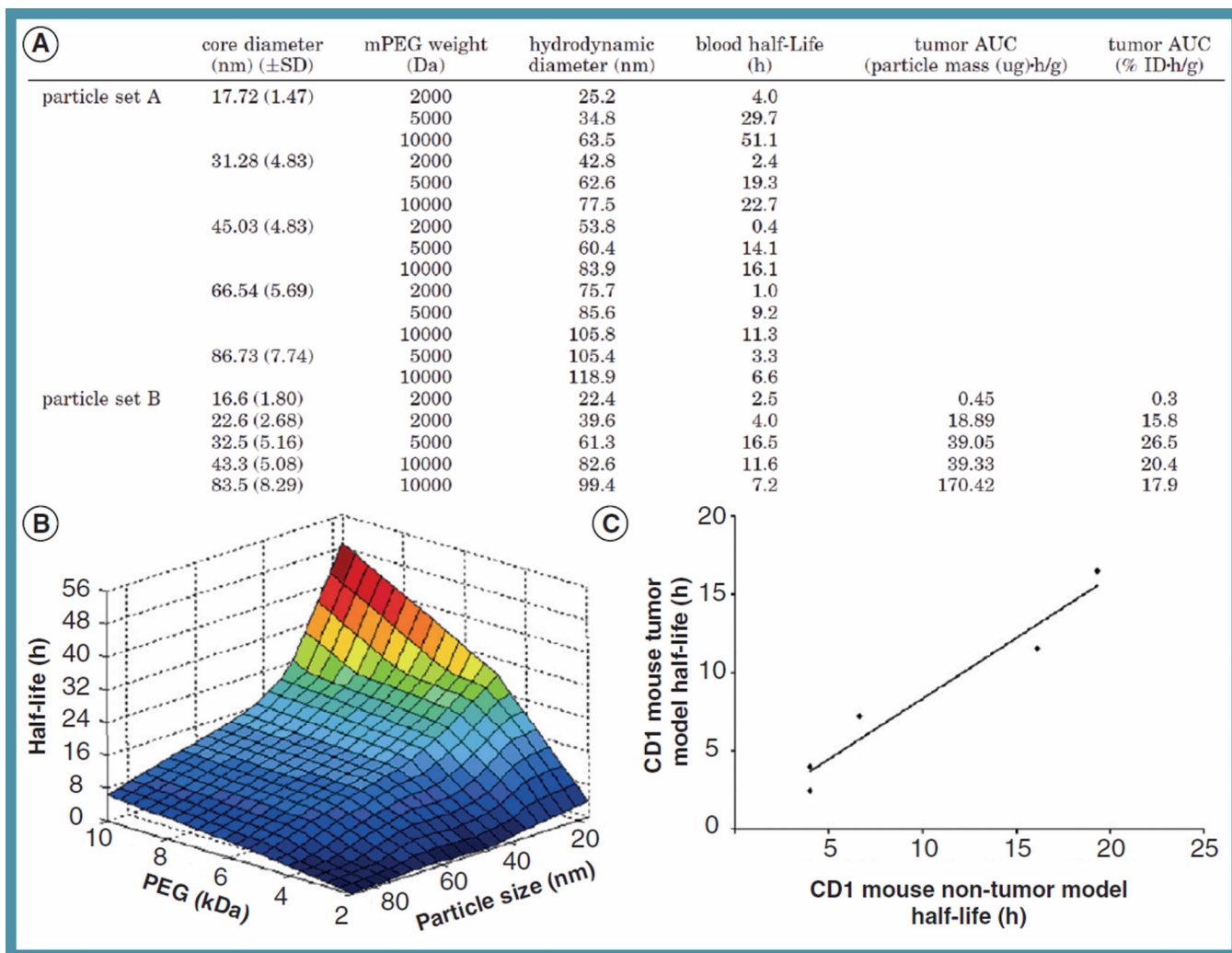
	core diameter (nm) (±SD)	mPEG weight (Da)	hydrodynamic diameter (nm)	blood half-Life (h)	tumor AUC (particle mass (ug)·h/g)	tumor AUC (% ID·h/g)
particle set A	17.72 (1.47)	2000	25.2	4.0		
		5000	34.8	29.7		
		10000	63.5	51.1		
	31.28 (4.83)	2000	42.8	2.4		
		5000	62.6	19.3		
		10000	77.5	22.7		
	45.03 (4.83)	2000	53.8	0.4		
		5000	60.4	14.1		
		10000	83.9	16.1		
	66.54 (5.69)	2000	75.7	1.0		
		5000	85.6	9.2		
		10000	105.8	11.3		
	86.73 (7.74)	5000	105.4	3.3		
		10000	118.9	6.6		
particle set B	16.6 (1.80)	2000	22.4	2.5	0.45	0.3
	22.6 (2.68)	2000	39.6	4.0	18.89	15.8
	32.5 (5.16)	5000	61.3	16.5	39.05	26.5
	43.3 (5.08)	10000	82.6	11.6	39.33	20.4
	83.5 (8.29)	10000	99.4	7.2	170.42	17.9

Figure 4. Pharmacokinetics of PEGylated Au nanoparticles
(A) Relationship between circulatory half-lives, hydrodynamic diameter and tumor accumulation for spherical Au nanoparticles of varying size and thiolated PEG surface stabilizer molecular weight. **(B)** The circulatory half-lives of PEGylated Au nanospheres are inversely proportional to particle size and PEG molecular weight (for particles >16-nm core diameter). **(C)** The similar pharmacokinetics of PEGylated Au nanoparticles in tumor-bearing and nontumor-bearing mouse models.
PEG: Poly(ethylene glycol).
Reprinted with permission from [124]. © American Chemical Society (2009).
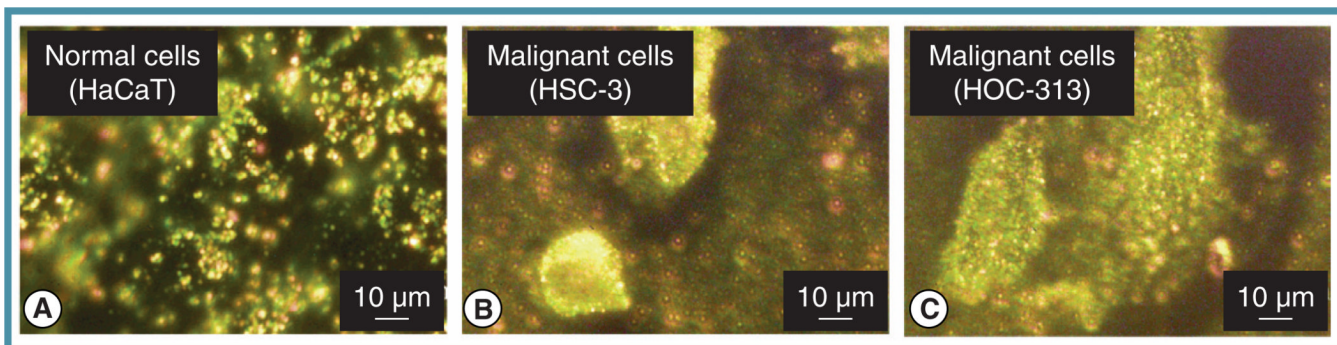
Figure 5. Selective biodiagnostic labeling of cell cultures using antibody–Au nanoparticle conjugates
(A) Nonmalignant HaCaT keratinocyte cells show only nonspecific labeling by Au nanospheres conjugated with antibodies for anti-EGFR. Malignant **(B)** HSC-3 and **(C)** HOC-313 squamous cell carcinoma cells show high binding with anti-EGFR Au nanoparticles due to their characteristically high cell-surface EGFR expression levels. Reprinted with permission from [136]. © American Chemical Society (2005).
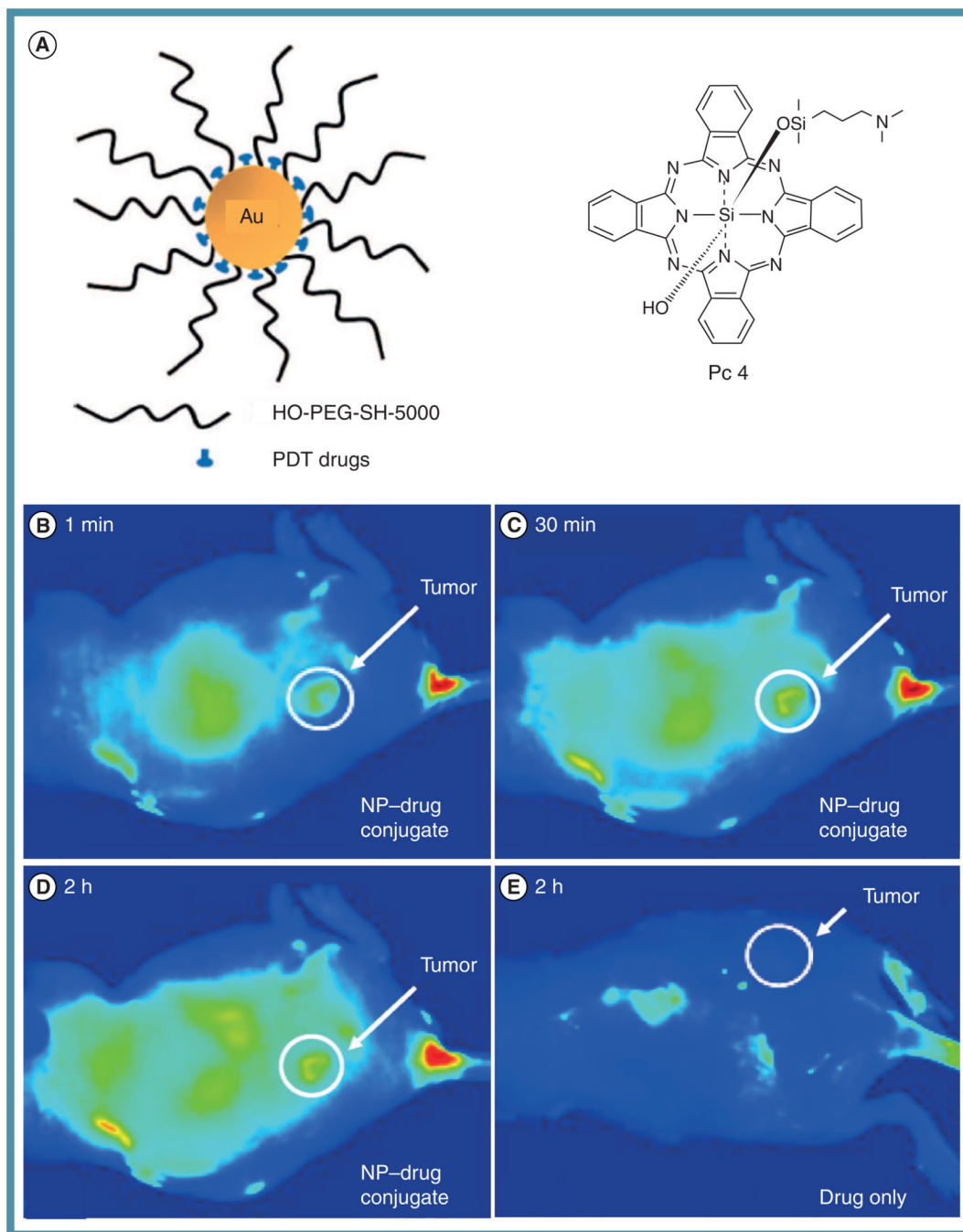
Figure 6. Conjugation and *in vivo* tumor accumulation of a photodynamic therapy photosensitizer–Au nanoparticle conjugate
(A) AuNPs were functionalized with Pc4 photosensitizer through Au–N bond formation at the terminal amine group on the Pc4's axial ligand. Fluorescence images of a tumor-bearing mouse at **(B)** 1 min, **(C)** 30 min and **(D)** 2 h after intravenous injection with Pc4–AuNPs. Fluorescence from Pc4 molecules indicated efficient delivery and accumulation of the drug in the rear flank tumor site (white circle). **(E)** Mice injected only with Pc4 exhibited no appreciable drug circulation or tumor-specific accumulation.
AuNP: Au nanoparticle; NP: Nanoparticle; PDT: Photodynamic therapy; PEG: Poly(ethylene glycol).

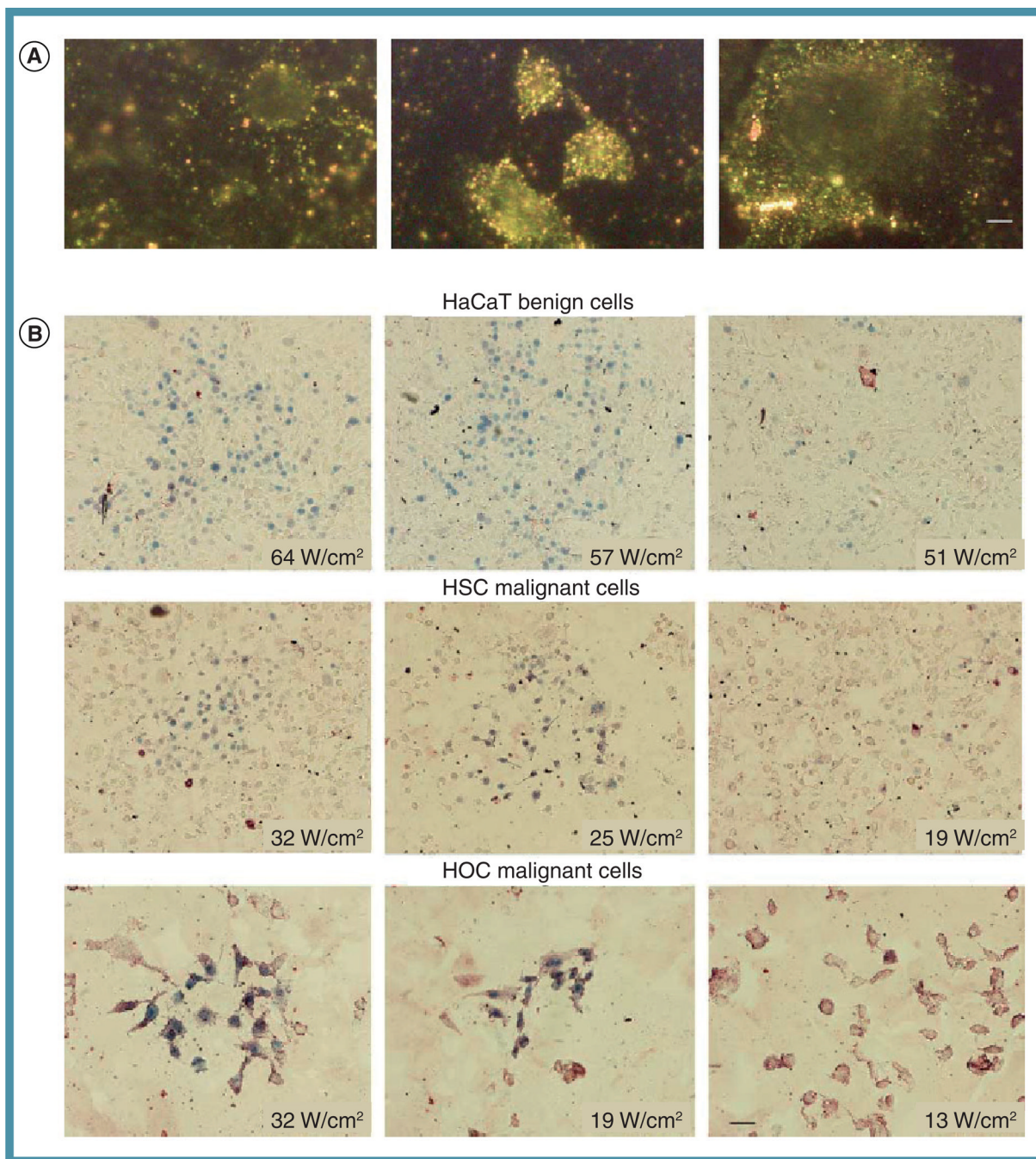Reprinted with permission from [153]. © American Chemical Society (2008).

Figure 7. Selective targeting and *in vitro* near-IR plasmonic photothermal therapy of cancerous and noncancerous cell lines
(A) Au nanorods conjugated with antibodies to anti-EGFR showed increased labeling of HSC-3 and HOC malignant cell lines which overexpress EGFR, whereas nonmalignant cells remained unlabeled. **(B)** Near-IR laser exposure at various laser powers revealed that malignant cell lines were killed at and above 19 W/cm^2 while nonmalignant cell lines required 57 W/cm^2.
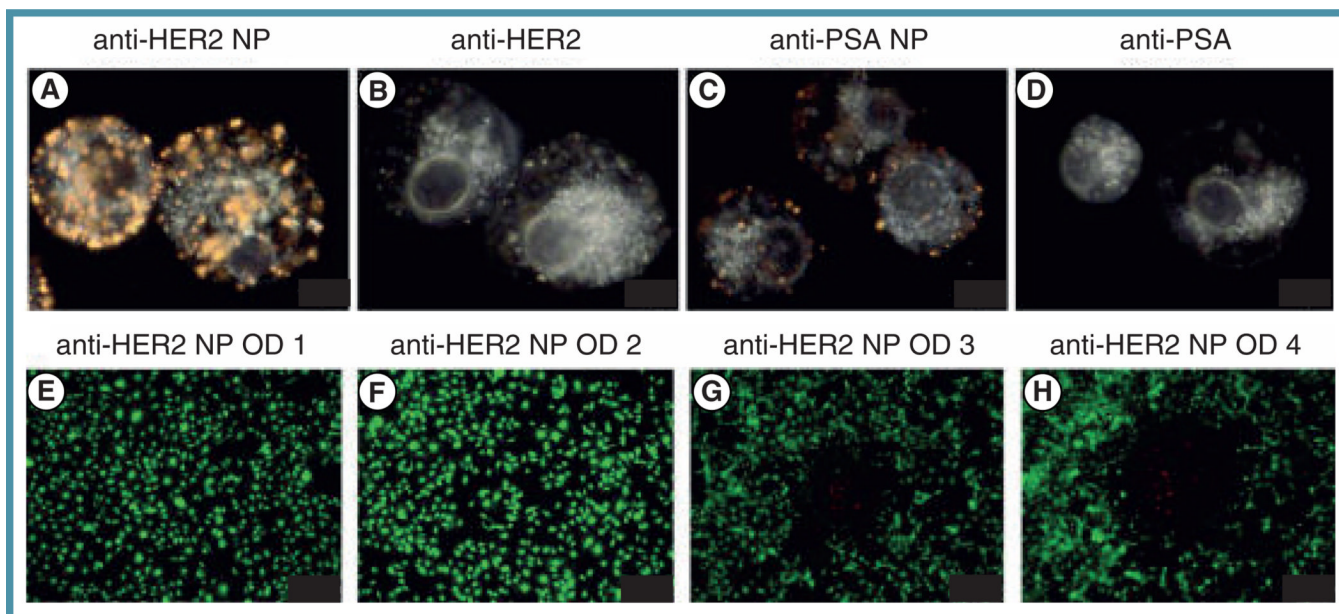Reprinted with permission from [157]. © Elsevier (2006).

Figure 8. *In vitro* **near-IR photothermal therapy using nanobody-conjugated branched Au nanoparticles**
Specific labeling of SKOV3 cells was achieved using **(A)** HER2 antibody (anti-HER2) and **(C)** PSA antibody (anti-PSA) Au–NP conjugates. Non-conjugated **(B)** anti-HER2 and **(D)** anti-PSA exhibited no image contrast. **(E–H)** Near-IR laser (continuous wave, 690 nm, 38 W/cm^2) treatment for 5 min showed increased cell death with increasing incubation concentration of anti-HER2-Au NPs.
NP: Nanoparticle; OD: Optical density (concentration); PSA: Prostate-specific antigen.
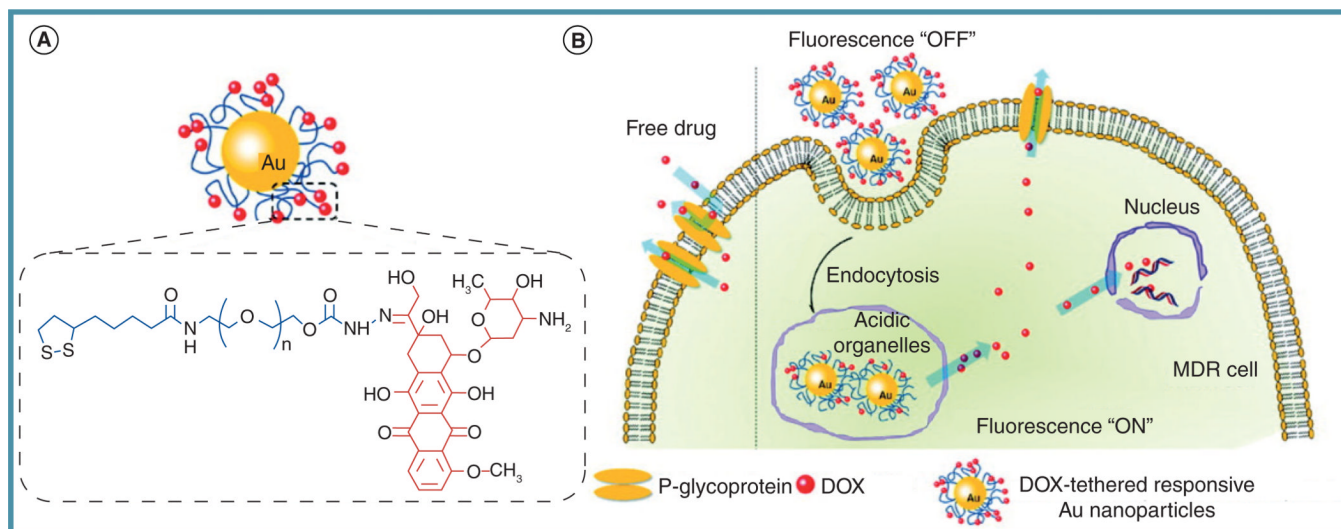Reprinted with permission from [158]. © American Chemical Society (2011).

Figure 9. Internalization and delivery of the chemotherapeutic drug doxorubicin in multidrug-resistant breast cancer cells through conjugation with Au nanoparticles
(A) Au nanoparticles were functionalized with DOX through an acid-liable poly(ethylene glycol) linker. **(B)** DOX-Au nanoparticles enter the cell through endocytosis and subsequently released the conjugated drug once in the acidic endo/lysosomal environment. Drug release, here, can be monitored using DOX fluorescence, which becomes de-quenched upon released from the Au nanoparticle.
DOX: Doxorubicin; MDR: Multidrug resistance.
Reprinted with permission from [162]. © American Chemical Society (2011).